Transduction catalysis: doxorubicin accelerates and enhances rAAV-mediated gene expression in the cortex of mouse, cat and monkey

Hongliang Gong[1,2], Nini Yuan[1], Zhiming Shen[1], Cheng Tang[1,2], Stewart Shipp[1], Liling Qian[1], Yiliang Lu[1], Ian Max Andolina[1], Shenghai Zhang[4], Jihong Wu[4], Hui Yang[1,2,3], Wei Wang[1,2,3,5*]

[1] Institute of Neuroscience, the Center for Excellence in Brain Science and Intelligence Technology, State Key Laboratory of Neuroscience, Key Laboratory of Primate Neurobiology, Chinese Academy of Sciences, Shanghai 200031, China

[2] School of Future Technology, University of Chinese Academy of Sciences, Beijing 100049, China

[3] Shanghai Center for Brain and Brain-Inspired Intelligence Technology, Shanghai 200031, China

[4] Department of Ophthalmology, Eye and ENT Hospital of Fudan University, Shanghai 200031, China

[5] Lead Contact

* Correspondence to: w.wang@ion.ac.cn

SUMMARY

Rapid and efficient gene transduction via recombinant adeno-associated viruses (rAAVs) is highly desirable across many basic and clinical research domains. Here we report vector co-infusion with doxorubicin, a clinical anti-cancer drug, markedly enhanced rAAV-mediated gene expression in cerebral cortex across mammalian species (cat, mouse, and macaque), acting throughout the time-period examined and detectable at just three days post-transfection. This enhancement showed serotype generality, being common to rAAV serotypes 2, 8, 9 and PHP.eB tested, and was observed both locally, and at remote locations consistent with doxorubicin undergoing retrograde axonal transport. All these effects were observed at doses matching human blood plasma levels in clinical therapy, and lacked detectable cytotoxicity as assessed by cell morphology, activity, apoptosis and behavioral testing. Altogether, this study identifies an effective means to improve the capability and scope of *in vivo* rAAV applications, accelerating and augmenting gene transduction at doxorubicin concentrations paralleling medical practice.

Highlights:

1. Anti-cancer drug doxorubicin doubles the rate of rAAV-mediated transgene expression
2. Doxorubicin enhancement generalizes across rAAV serotypes and animal species
3. The effect is observed in both locally and retrogradely infected cortical neurons
4. The effective dosage is free from cytotoxicity and matches clinical settings

INTRODUCTION

The manipulation of gene expression in specific populations of neurons is a potent capability for both neuroscientific research (Betley and Sternson, 2011; Sun and Schaffer, 2018) and therapeutic intervention in genetic disorders (Naldini, 2015). Vectors derived from adeno-associated virus (AAV) are especially favored for *in vivo* gene manipulation as they provide a non-pathogenic and minimally immunogenic means to achieve persistent, stable transgene expression within the mammalian central nervous system (CNS) (Hudry and Vandenberghe, 2019; Kaplitt et al., 1994). Combined with molecular genetic techniques, recombinant AAV (rAAV) has proved to be a powerful research tool, widely used in gene editing and expression modulation (Atasoy et al., 2008; Ran et al., 2015), neuronal morphology mapping (Parekh and Ascoli, 2013), *in vivo* imaging (Tian et al., 2009), neural circuit analysis (Cruz-Martin et al., 2014; Zhang et al., 2016) and treatment of neurological disorders (Deverman et al., 2018; Hudry and Vandenberghe, 2019; Kaplitt et al., 1994). Unhelpfully, however, the expression of genes transduced via rAAV undergoes a prolonged lag phase (≥ two weeks) before reaching significant levels for intervention (Diester et al., 2011; Peel et al., 1997). This delay in expression limits the utility of rAAV applications in both experimental and clinical practice, for example in brain development studies during critical and sensitive periods (e.g., neuronal migration, circuit formation and synaptic refinement) (Krol and Feng, 2018; Meredith, 2015), and in the treatment of diseases that requires timely intervention to forestall irreversible tissue damage (e.g., ischemic brain injury) (Sehara et al., 2018). Thus a more effective means to induce rapid and high-level rAAV vector transduction and expression in mammalian CNS is in much need of development.

Previous research efforts have aimed to improve the vector system, i.e. the viral capsid and genome. By utilizing natural isolates with different tropisms, new rAAV variants with superior efficacy have been engineered through capsid transformation (Broekman et al., 2006), amino acid mutation (Zhong et al., 2008), domain/subunit swapping (Rabinowitz et al., 2004), or screened from mutant capsid libraries (Deverman et al., 2016; Maheshri et al., 2006; Yang et al., 2009). At the level of the vector genome, the vector expression cassette has been optimized with stronger promoters, enhancers, and more effective polyadenylation sequences (Monahan et al., 2015; Peel et al., 1997). An alternative strategy has been the development of a self-complementary (scAAV) vector to bypass second-strand DNA synthesis and so enhance the rapidity of gene transduction, at the cost of halving the payload capacity (McCarty et al., 2003; McCarty et al., 2001). Combined with advances in delivery techniques, good progress has been achieved in respect of transduction efficiency in small animals (Chan et al., 2017). However, for mammals with large brains, particularly non-human primates and humans, the challenge is to achieve consistent, high levels of transduction across volumetrically extensive, but specific brain structures. This problem is manifest in therapeutic trials, e.g. where rAAV is targeted to the putamen (Hadaczek et al., 2010; Hwu et al., 2012) and in research applications, e.g. where

addressing insufficient transduction by vector readministration encounters a heightened immune response (Mendoza et al., 2017). Furthermore the delay in expression remains critically important, since scAAV can only be used for smaller transgenes (less than 2.2 kb) (McCarty et al., 2001; Wang et al., 2019).

The application of exogenous agents is a new strategy to promote rAAV transduction in the CNS. Early studies revealed that techniques such as adenovirus co-infection, ionizing radiation and genotoxic agents can all promote rAAV2 transduction, inducing faster and higher gene expression in cultured cells (Alexander et al., 1994; Ferrari et al., 1996; Fisher et al., 1996; Kanazawa et al., 2001). Similar promotion was also achieved with chemical agents that damage DNA, inhibit topoisomerase activity, or modulate proteasome function (Nicolson et al., 2016; Prasad et al., 2007; Russell et al., 1995; Yan et al., 2004). These agents appear to promote viral intracellular trafficking and/or second-strand DNA synthesis, two rate-limiting steps in rAAV transduction that see little improvement with vector capsid engineering. However, severe side-effects have hindered their application *in vivo,* calling for alternative drugs or strategies that are less cytotoxic. ***Doxorubicin*** is a frontline drug that has been widely used in cancer therapy (Tacar et al., 2013). As a known inhibitor of topoisomerase, it can also modulate proteasome function and thus has clear potential to promote rAAV transduction. That doxorubicin enhances rAAV2 transduction was initially reported in human airway epithelial cell lines (Yan et al., 2004), followed by tests in cultured neuronal cells (Zhang et al., 2009) and retinal pigment epithelium cells (Zhang et al., 2012). However, for *in vivo* applications in the CNS, it is crucial to examine the precise time-course of neural transduction or the dose-dependency of the longer term balance between efficacy and neurotoxicity. It was thus our goal to determine just how effectively doxorubicin might accelerate rAAV-mediated gene transduction in mammalian CNS and establish the ceiling for toxicity. Furthermore, it is unarguably important to determine the universality of the action of doxorubicin across a range rAAV serotypes, brain structures, and mammalian species.

Here, we have systematically evaluated the effect of doxorubicin on transgene expression in the cerebral cortex of mice, cats, and macaque monkeys, by intraparenchymal administration of doxorubicin in combination with different rAAV serotypes (rAAV8, rAAV2, rAAV9 and rAAV-PHP.eB). We found that doxorubicin greatly enhanced transgene expression mediated by every rAAV vector that we tested, differing little between species. Across subjects, doxorubicin took almost immediate effect and continued to act throughout the time period examined. Dose escalation test showed that the effect of doxorubicin on rAAV transduction was concentration-dependent, and was mediated with negligible adverse side-effects at doses well below tolerance. Finally, we demonstrated the practicality of doxorubicin-promoted rAAV transduction for two specific experimental applications, namely *in vivo* two-photon imaging in mouse visual cortex, and retrograde tracing of inter-areal connections with rAAV2-retro in macaque visual cortex. In sum, our findings offer a feasible strategy

that can complement vector system optimization for rapid and efficient *in vivo* rAAV transduction in the CNS across species.

RESULTS

Doxorubicin Enhances rAAV Transduction with No Impact upon Cell Tropism

We began by evaluating the effect of doxorubicin in the cerebral cortex of cat, a well-studied mammalian model (Vite et al., 2003). For our standard vector we selected rAAV8, a serotype isolated from rhesus monkey with the express aim of developing a vector for gene therapy with minimal immunogenicity in human tissues (Gao et al., 2002). rAAV8 proved to have a CNS transduction capability superior to that of rAAV2 when introduced into the cerebral vesicles of neonatal mice (Broekman et al., 2006) and was also shown to mediate efficient gene transfer after intraparenchymal injection in various cortical and subcortical structures of primate brains (Gilkes et al., 2016; Masamizu et al., 2010; Masamizu et al., 2011). rAAV8-hSyn-EGFP (titer: 1×10^{12} vg/ml, 1 μl per injection), a rAAV8 vector which encoded green fluorescent protein (GFP) under a neuron-specific promoter hSyn, was administered via stereotactic injection into extrastriate visual cortex of three cats, combined with doxorubicin (10 μg/ml) in one hemisphere and vector alone (as a control) in the other (**Figure 1A**). Thirty days after injection animals were sacrificed and the expression of GFP determined with standard histological techniques (see Methods). The results from an example case are shown in **Figure 1B-D**. Fluorescence images revealed that pressure-injection of vector solution led to focal transduction within a radius of 750 μm from the injection syringe-track, with local GFP expression in cell bodies and axons that projected to extrinsic structures. Compared with the control group, GFP fluorescence in the doxorubicin-treated group was noticeably brighter (**Figure 1C)**; image quantification showed that its intensity was significantly increased (~2.5-fold) by doxorubicin (405.5 ± 46.1 *vs* 1015 ± 58.4, $p < 0.0001$**,** two-tailed t-test; **Figure 1C**). Consistent with studies in mouse and marmoset (Watakabe et al., 2015), rAAV8-mediated GFP expression was not homogeneous across cortical layers, with layer 4 the weakest. We quantified the proportion of transduced neurons in equivalent regions of interest within the doxorubicin and control injection sites, as indicated by neuronal-specific marker NeuN (**Figure 1D**). Confocal images revealed that the proportion of GFP-expressing neurons was markedly increased, exhibiting higher fluorescence across all cortical layers when treated with doxorubicin (layer 2/3: 93 ± 3% versus 82 ± 3%; layer 4: 79 ± 3% versus 41 ± 5%; layer 5: 92 ± 2% versus 78 ± 3%; layer 6: 92 ± 2% versus 75 ± 4%; all $p < 0.01$, two-tailed t-test; **Figure 1D**). Across all layers the average ratio of GFP-positive neurons was 91 ± 2% in the doxorubicin-treated group, compared with 70 ± 3% in the control group ($p < 0.001$, two-tailed t-test; Figure 1D). Yet more notably, after a tenfold decrease of vector (titer: 1×10^{11} vg/ml, 1 μl per injection), doxorubicin treatment still gave an equivalent level of GFP expression to the control (titer: 1×10^{12}

vg/ml, 1 μl per injection) (401.3 ± 32.8 *vs* 405.5 ± 46.1, p = 0.7211, two-tailed t-test).

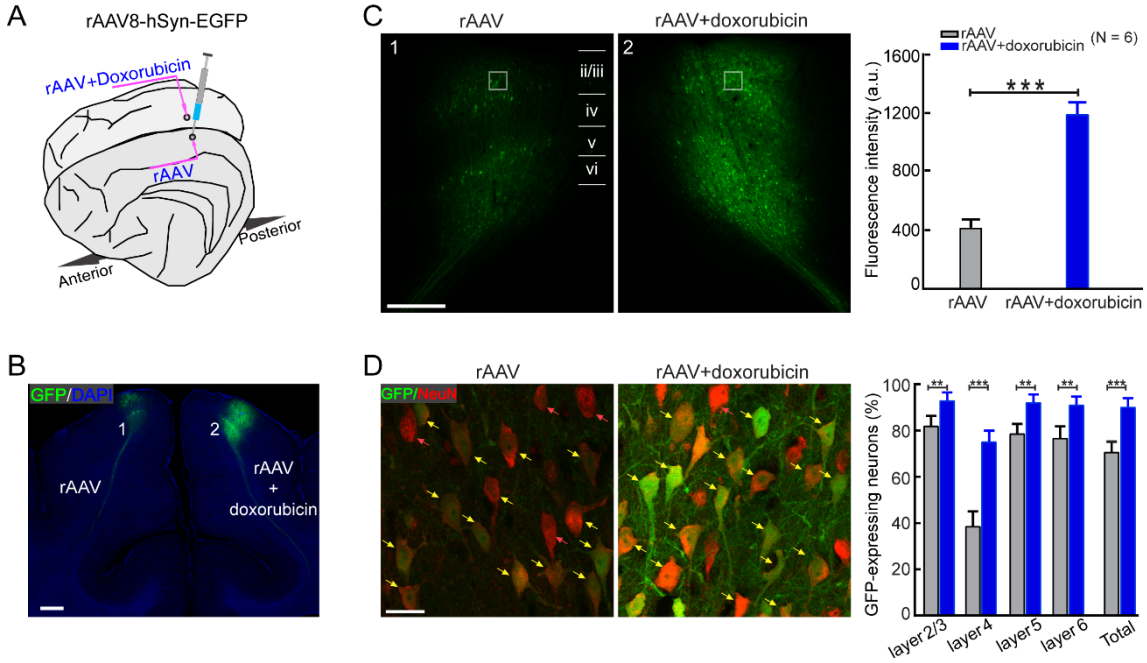

Figure 1. Doxorubicin Promotes rAAV8-Mediated Gene Transduction in Cat Visual Cortex

(**A**) Schematic representation of injections. Small quantities of rAAV8-hSyn-EGFP (titer: 1×10^{12} vg/ml, 1 μl per injection) were delivered into the left and right hemisphere of cat visual cortex, vector alone or coupled with doxorubicin (10 μg/ml). (**B**) Coronal sections from visual cortex of an example cat injected with rAAV8 (left) and rAAV8-plus-doxorubicin (right). Blue, DAPI; green: GFP. Scale bar, 1 mm. (**C**) Cortical fluorescence intensity comparison between rAAV8 and rAAV8-plus-doxorubicin after 30 days of expression. Scale bar, 500 μm. (**D**) Left: confocal images of GFP expression and NeuN staining of layer 2/3, as indicated by the white boxes in **C**. Neurons are identified by immunohistochemistry of NeuN antibody. Transduction efficiency is assessed by colocalization of GFP and NeuN marker (yellow arrow). Scale bar, 25 μm. Right: quantification of the percentage of neurons transduced across cortical layers. Neurons in layer 4 showed the weakest GFP expression. For quantification in **C** and **D**, n = 6 injections from 3 cats per group, mean ± s.e.m.; two-tailed t-test (*p <0.05, **p <0.01, ***p <0.001.)

To determine whether the effect of doxorubicin on rAAV transduction is exclusive to neurons, we replaced hSyn with the ubiquitous promoter CAG. The modified vector, rAAV8-CAG-EGFP (titer: 5×10^{11} vg/ml, 1 μl per injection) was administered with or without doxorubicin (10 μg/ml). The phenotypes of transduced cells were then determined by immunohistochemical detection of cell-type-specific markers, i.e. NeuN for neurons, glial fibrillary acidic protein (GFAP) for astrocytes and ionized calcium binding adaptor molecule (Iba-1) for microglia (**Figure S1A-C**). As anticipated, we found that under the control of CAG promoter GFP was expressed not only in neurons (**Figure S1A**) but also in astrocytes (**Figure S1B**); fluorescence intensity (**Figure S1D**) and the proportions of both GFP-positive neurons and astrocytes were significantly increased at the injection sites of the doxorubicin-treated group relative to the control (neuron: 41 ± 4% versus 21 ± 6%; astrocyte: 32 ± 6% versus 14 ± 4%; $p < 0.05$, two-tailed t-test; **Figure S1E**). With or without doxorubicin, there was no detectable signal in microglia (**Figure S1C and 1E**), consistent with experience to date that this cell class is relatively refractory to transduction by AAV (Maes et al., 2019). These results suggest that doxorubicin treatment enhances gene transduction mediated by rAAV8 in the CNS, with no

quantitative impact upon its cellular tropism, which is governed by the vector's capsid (Srivastava, 2016).

Doxorubicin Accelerates rAAV-Mediated Gene Expression

Practical, rapid onset of rAAV-mediated gene expression is highly significant in regard to studies of brain development, as well as neurodevelopmental and degenerative diseases where timely intervention should precede the onset of irreversible tissue damage (Candolfi et al., 2010; Krol and Feng, 2018; Shimazaki et al., 2000). To explore the impact of doxorubicin on the onset of rAAV transduction in the CNS, we carefully examined the time course of transgene expression in doxorubicin-treated versus control groups. Following our established procedure, rAAV8-hSyn-EGFP (titer: 1×10^{12} vg/ml, 1 μl per injection) alone or coupled with doxorubicin (10 μg/ml) was administered to cat visual cortex, and the expression levels of GFP were determined with standard histological techniques at 3, 7, 15 and 30 days following injection (**Figure 2A**). We found that the pace of transgene expression was greatly accelerated in the presence of doxorubicin. In the control group, GFP fluorescence could be detected no earlier than 7 days post-injection. This reduced to 3 days for the doxorubicin-treated group, with a steady increase in GFP expression thereafter. At 7 days after injection, GFP activity in the doxorubicin-treated group was about four-fold higher than that in the control group (104.3 ± 9.6 *vs* 25.2 ± 2.5, $p = 0.0003$, two-tailed t-test), actually matching the 15-day level of the control group (104.3 ± 9.6 *vs* 118.7 ± 18.9, $p = 0.5157$, two-tailed t-test). Throughout the period of examination, the level of GFP expression in the doxorubicin-treated group consistently exceeded the control group (3 days: $p = 0.0015$; 7 days: $p = 0.0003$; 15 days: $p < 0.0001$; 30 days: $p < 0.0001$; two-tailed t-test; **Figure 2B**). These results reveal that doxorubicin significantly accelerates rAAV transduction, facilitating timely interventions in the CNS by means of rapid and efficient transgene expression.

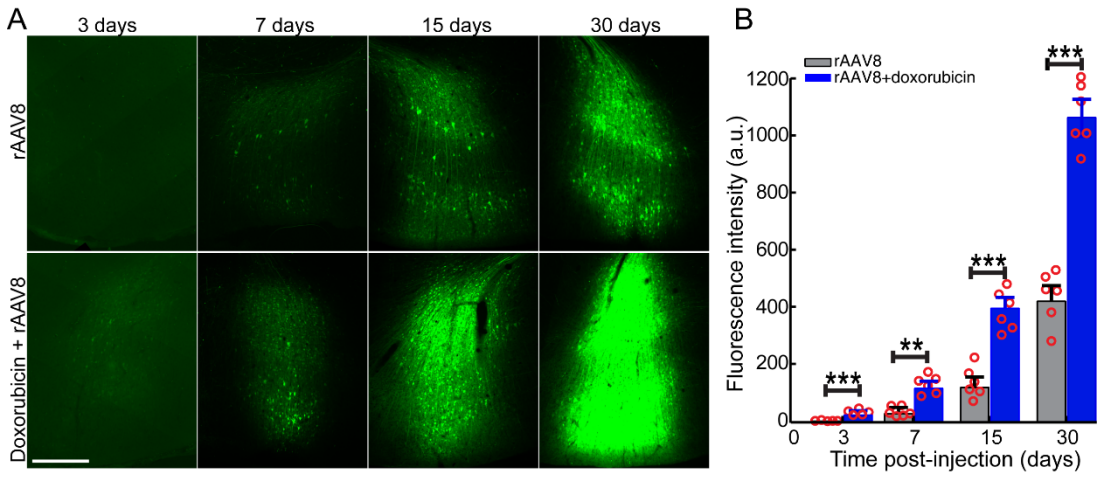

Figure 2. Doxorubicin Accelerates rAAV8-Mediated Gene Expression in The Cerebral Cortex
(**A**) Representative GFP expression in cat cortex after an injection of rAAV8 with doxorubicin or vector alone at the specified time points. rAAV8-hSyn-EGFP vector (titer: 1×10^{12} vg/ml, 1 μl per injection) was administered into cat

visual cortex alone or combined with doxorubicin (10 μg/ml) and GFP intensities were assessed with histological techniques at varied intervals post-injection. The gamma value was adjusted equally to enable the visualization of GFP signals in both doxorubicin-treated and control conditions at 3 days. Scale bar, 500 μm. (**B**) Quantification of GFP intensity at these same time points after infection. For 7, 15 and 30 days, n = 6. For 3 day, n=5; mean ± s.e.m; two-tailed t-test (*p <0.05, **p <0.01, ***p <0.001.)

Dose-Dependency for Doxorubicin Enhancement of rAAV-Mediated Gene Expression

Previous *in vitro* studies have indicated that the enhancement of rAAV2 transduction by doxorubicin is dose-dependent, and takes effect at sub-clinical concentrations (Zhang et al., 2012). An equivalent *in vivo* study is essential to determine the optimal dosage of doxorubicin for neurological administration, a balance between efficacy for rAAV transduction versus toxicity to neural tissues. Again, using the rAAV8-hSyn-EGFP vector (titer: 1×10^{12} vg/ml, 1 μl per injection), seven different concentrations of doxorubicin (range 0.1-100 μg/ml) plus an eighth control were infused into the cerebral cortices of six cats. GFP expression was examined in brain sections with fluorescence microscopy seven days post-injection. The evident dependency of GFP expression levels upon doxorubicin concentration can be seen in Figure 3A, displaying a steady increase within the range of 0.1 to 30 μg/ml. To mitigate doxorubicin concentration loss through diffusion, GFP intensity was measured within a ROI (500 x 1000 μm) at the core of each injection, as indicated in the control (**Figure 3A**). Quantitative results confirmed the dose-dependent increase of rAAV-mediated GFP expression by doxorubicin, with the maximal increase obtained at 30 μg/ml (ANOVA $F = 53.8$, $p < 0.0001$, post hoc Tukey Kramer correction: control *vs* 1.0 μg/ml, $p = 0.02$; control *vs* 3.0 μg/ml, $p = 0.008$; control *vs* 10 μg/ml, $p = 0.002$; control *vs* 30 μg/ml, $p = 0.0012$; **Figure 3B**). For the topmost doxorubicin dosage of 100 μg/ml, GFP intensity decreased sharply at the core of injection site, hence demonstrating notable cytotoxicity at this high concentration.

To further substantiate the differential dose-effect of doxorubicin, we analyzed the status of GFP-expressing neurons with the nuclear marker DAPI and the neuron-specific marker NeuN (**Figure 3C-F**). Confocal images revealed that cell bodies and neurites of infected neurons exhibited intact and normal morphology after doxorubicin treatment at a dosage from 0.1 to 10 μg/ml. At a dose of 30 μg/ml the neurites of neurons in the core of injections diminished, and cell bodies became round with weak or even absent NeuN signals. When doxorubicin concentration reached 100 μg/ml neurons were completely absent from the core of the injection, with glial accumulations in their place. These data further informed the dose-dependency of the enhancement of rAAV-mediated gene transduction by doxorubicin in the CNS, indicating that, at a dose of up to 10 μg/ml, gene expression is notably enhanced by doxorubicin with negligible cytotoxicity – at least insofar as cat visual cortex is representative of mammalian CNS tissues.

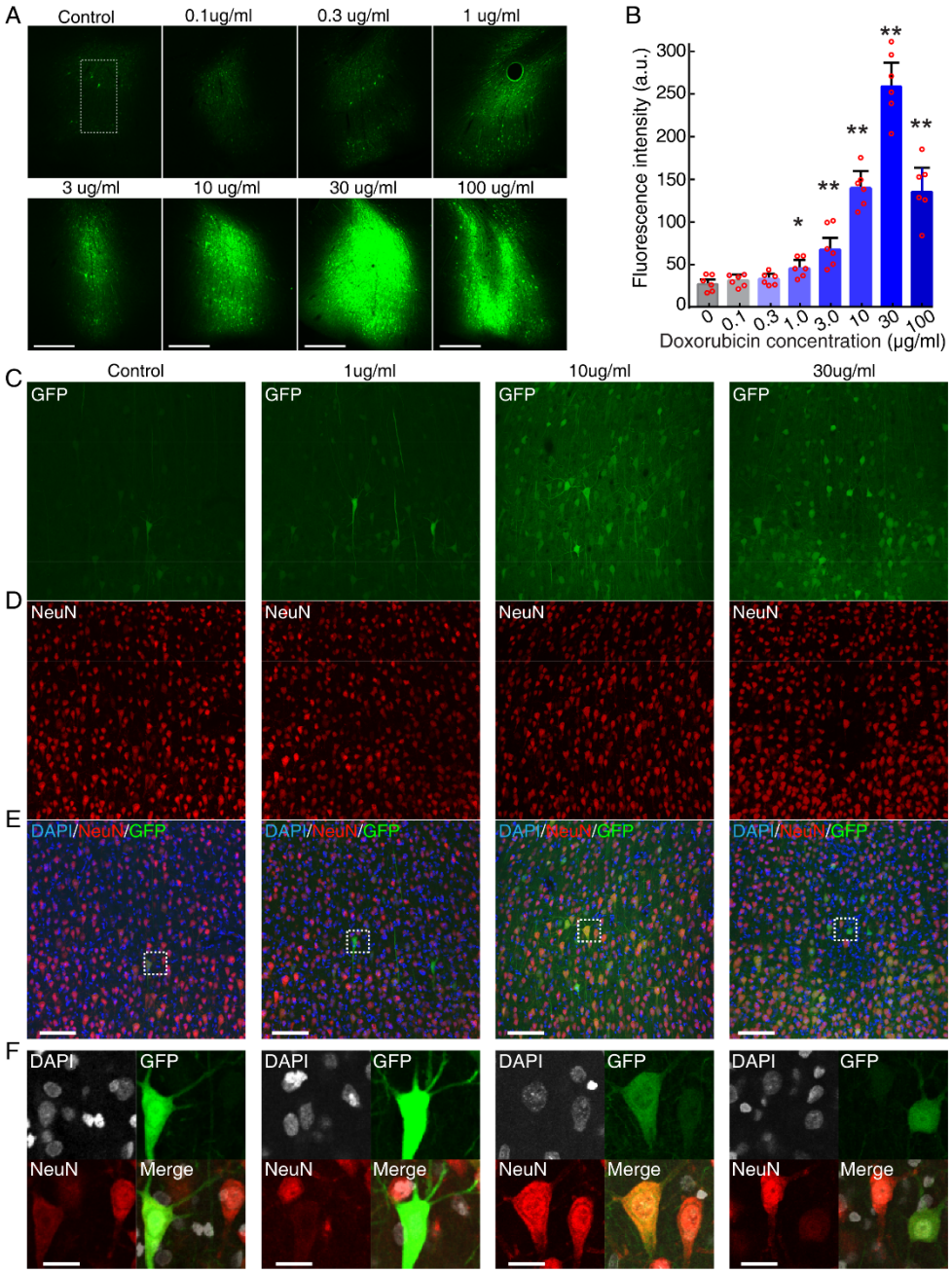

Figure 3. The Effect of Doxorubicin on rAAV Transduction Is Concentration-Dependent, and Free from Appreciable Cytotoxic Effects at a Dosage from 1 to 10 μg/ml

(**A**) Representative fluorescence images of injections 7 days after co-administration of rAAV8-hSyn-EGFP (titer: 1×10^{12} vg/ml, 1 μl per injection) with different concentrations of doxorubicin. Scale bar, 500 μm. (**B**) Quantification of core fluorescence intensity with doxorubicin at different concentrations, as indicated in A. For quantification: n = 6 injections per group, mean ± s.e.m. ANOVA, post hoc Tukey Kramer correction, *$p < 0.05$, **$p < 0.01$, ***$p < 0.001$. (**C-E**) Status of transduced neuronal cells (GFP, green) at cellular level (**C**), quantified by neural marker NeuN (red) (**D**), and nuclear marker DAPI (blue) (**E**). Scale bar, 100 μm. (**F**) Magnified views of neuronal cells under different doxorubicin concentrations (as indicated in the inset of **E**). Scale bar, 20 μm.

Locally Injected Doxorubicin Lacks Detectable Cytotoxicity for Neural Tissue

Doxorubicin is a frontline chemotherapeutic drug, used to restrict cell division in clinical treatment of tumors. Its cytotoxicity is mainly specific to dividing cells, as it takes effect by inhibiting cellular DNA replication and inducing cell apoptosis (Tacar et al., 2013). There is also notable cardiotoxicity

at high-dose schedules (Levis et al., 2017), but for neurological administration at lower concentrations to non-dividing cells, these adverse effects should be minor. Nevertheless, it remains important to determine whether doxorubicin has cytotoxic effects upon neural tissues under experimental conditions.

We used the well-established TUNEL assay (that detects the DNA breaks marking the terminal phase of apoptosis) and immunocytochemistry to assess neuronal apoptosis consequent to doxorubicin application. Seven days after administration of 10 μg/ml doxorubicin, TUNEL staining was performed on brain sections and apoptotic cells were screened by confocal fluorescence microscopy. As presented in Figure 4A, no appreciable apoptotic effect was observed in either the doxorubicin-treated group or the control group (rAAV alone), when compared to a positive control treated with DNase I, as indicated by fluorescent-labeled nuclear marker DAPI (**Figure 4A**).

In addition to apoptosis, doxorubicin therapy can also cause inflammation, a major contributor to its cardiotoxicity and other side-effects (Sauter et al., 2011). To further establish the feasibility of doxorubicin treatment, the inflammatory response was examined by immunohistochemical detection of microglia, which generally aggregates in inflamed and necrotic tissues (Vela et al., 2002). After a similar interval, i.e. seven days following injection of 10 μg/ml doxorubicin, microglia were detected and counted in brain sections by antibody recognition of its specific marker Iba-1 (**Figure 4B**). Quantitatively, the outcome revealed no difference between the doxorubicin and control groups in regard to the expression of microglia after a single injection ($n = 5$, $p = 0.53$, two-tailed t-test; **Figure 4C**). Co-administration with rAAV8 gave a similar result, i.e. an rAAV-plus-doxorubicin group versus an rAAV group ($n = 5$, $p = 0.7$, two-tailed t-test; **Figure 4C**), indicating that there was no inflammatory response following a single injection of 10 μg/ml doxorubicin.

Finally, to determine whether doxorubicin treatment might induce any side effects at the behavioral level, we co-infused rAAVs with doxorubicin (10 μg/ml) or vector alone (as a control) into the primary motor cortex (M1) of mice in order to determine any consequent change in locomotor activity. 15 days post-injection the mice were placed in an open field chamber (40 x 40 cm) and allowed 15 minutes for free exploration (**Figure S2A**). Motor behavior was monitored by video camera (**Figure S2B**). None of the four movement parameters examined throughout the 15min period revealed any difference in behavior between doxorubicin-treated mice and the control: specifically, total distance traveled ($p = 0.28$; Wilcoxon rank-sum test; **Figure S2C**), mean velocity ($p = 0.28$; Wilcoxon rank-sum test **Figure S2D**), maximum velocity ($p = 0.43$; two-tailed t-test; **Figure S2E**) and time in movement (i.e. velocity ≥ 2 cm/s) ($p = 0.34$; two-tailed t-test; **Figure S2F**) were all equivalent. Taken together, these data show that local injection of doxorubicin lacks detectable adverse effects upon neural tissue under typical experimental conditions.

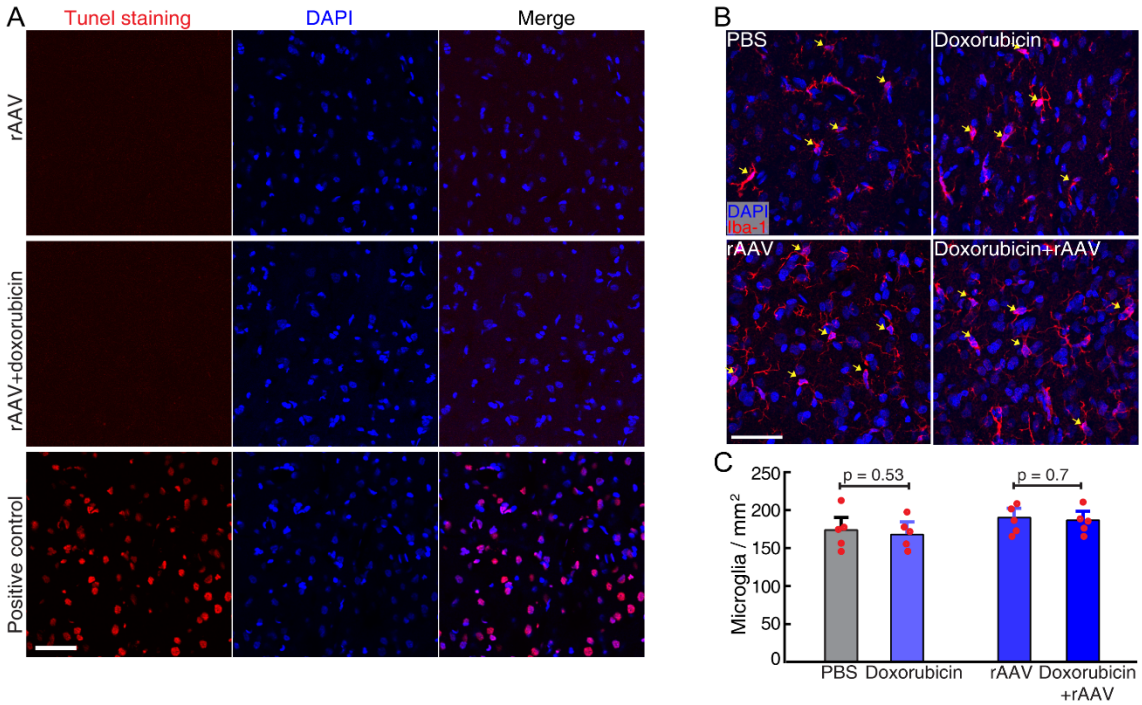

Figure 4. Doxorubicin Induces Little Appreciable Side Effects on Neural Tissue under the Experimental Conditions

(**A**) Confocal images of TUNEL stained sections after an injection of rAAV alone or combined with doxorubicin (10 μg/ml) and positive control samples pretreated with DNase I. Seven days following rAAV administration with or without doxorubicin, TUNEL staining and inflammatory response detection was performed on brain sections from each injection. blue, DAPI; red, apoptotic cell. Scale bar, 50 μm. (**B**) Representative images of fluorescent-labeled microglia cells (yellow arrows) by immunohistochemical detection of Iba-1; blue: DAPI, red: Iba-1. Scale bar, 50 μm. (**C**) Quantification of microglia cell numbers. n = 5, mean ± s.e.m., two-tailed t-test.

Doxorubicin Enhances rAAV Transduction Irrespective of rAAV Serotypes and Animal Species

AAV has multiple serotypes and new variants of rAAV are continually being developed for experimental and clinical purposes (Wang et al., 2019). To investigate how far our findings represent a general agonist effect of doxorubicin upon rAAV transduction, we employed two other rAAV serotypes: rAAV2 and rAAV-PHP.eB, the latter a variant of AAV9 selected to maximize transduction of mouse CNS via intravenous administration (Chan et al., 2017; Deverman et al., 2016). Combined with 10 μg/ml doxorubicin, viral vectors of rAAV2, rAAV8 and rAAV-PHP.eB expressing GFP under the CAG promoter were injected into cat cerebral cortex and GFP expression was assessed 7 days later. We observed similar levels of GFP expression in the control groups of rAAV8 and rAAV-PHP.eB, each significantly better than that achieved by rAAV2 (**Figure 5A**). More importantly, GFP expression was significantly upregulated by doxorubicin in all three serotypes of rAAV (rAAV2: $p = 0.006$; rAAV8: $p = 0.0094$; rAAV-PHP.eB: $p = 0.012$, two-tailed t test; **Figure 5A** and **5B**), suggesting doxorubicin indeed has a general agonist effect upon gene transduction mediated by rAAV vectors, irrespective of vector serotype.

We further tested the effect of doxorubicin in the cerebral cortex of different animal species. We infused rAAV-PHP.eB vector into the brain of mouse (visual cortex), cat (visual cortex) and macaque

monkey (motor cortex) and obtained substantial, quantifiable enhancement of transgene expression across all three species under the action of doxorubicin (**Figure 5C** and **5D)**. Qualitative examples of the enhancement of doxorubicin in macaque motor cortex are further shown in Figure S3A**.** The indication is that doxorubicin may well exert a general effect upon rAAV transduction, regardless of rAAV serotype and host species.

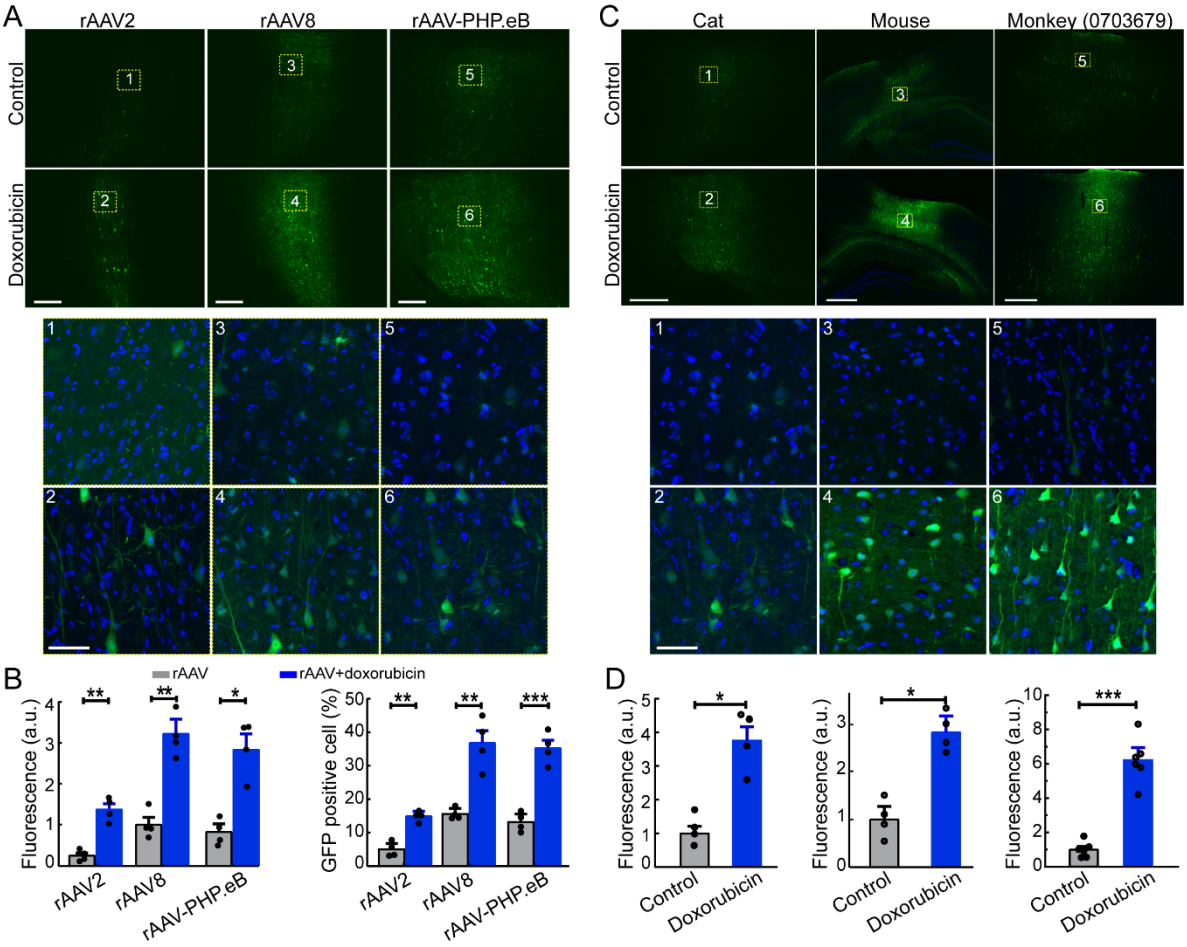

Figure 5. The Agonist Effect of Doxorubicin Is reproduced with Different rAAV Serotypes and Different Animal Species

(**A**) Representative images showing GFP expression via viral vectors of rAAV2, rAAV8 and rAAV-PHP.eB. Viral vectors of rAAV2, rAAV8 and rAAV-PHP.eB (a serotype 9 derivative) encoding GFP under the CAG promoter were injected either alone, or with 10 μg/ml doxorubicin, into cat cerebral cortex and GFP expression was assessed after 7 days. Upper panel: coronal slice through cat cerebral cortex injected with rAAV2, rAAV8 and rAAV-PHP.eB vector, respectively. Scale bar, 250 μm. Lower panel: magnified views of the injected areas, as indicated by numbers 1-6. DAPI: blue, GFP: green. Scale bar, 50 μm. (**B**) Quantification of mean GFP intensity (rAAV2, t = 5.80, p = 0.006; rAAV8, t = 4.16, p = 0.0094; rAAV-PHP.eB, t = 3.42, p = 0.012; two-tailed t-test) and percentage of transduced cells (rAAV2, t = 7.29, p = 0.0086; rAAV8, t = 5.45, p = 0.0094; rAAV-PHP.eB, t = 7.94, p = 0.0005; two-tailed t-test). (**C**) Representative images of vector injection-sites from cerebral cortex of cat, mouse and macaque monkey. rAAV-PHP.eB-CAG-EGFP vector was injected with 10 μg/ml doxorubicin and GFP protein was assessed after 7 days of expression. Lower panel: magnified views from the injected areas, as indicated by numbers 1-6. DAPI: blue, GFP: green. Scale bar, 500 μm (upper), 50 μm (lower). (**D**) Quantification of mean GFP intensity in cat (t = 3.42, p = 0.012), mouse (t = 4.69, p = 0.011) and monkey (t = 6.75, p = 0.0006). For quantification, n = 4 injections per group in cat and mice, and n = 6 injections per group from two monkeys; mean ± s.e.m. *p <0.05,**p <0.01. ***p <0.001.

Doxorubicin Enables Rapid Gene Transduction for *In Vivo* Two-Photon Imaging

Two-photon imaging has been a powerful tool widely used across many fields including: physiology (Cahalan and Parker, 2008), neurobiology (Denk et al., 1990; Svoboda and Yasuda, 2006), embryology (Squirrell et al., 1999) and tissue engineering (Rubart, 2004). Exploiting rAAV vectors carrying genetically encoded indicators, two-photon Ca^{2+} imaging has lent insight into the structural dynamics and functional activity of neuronal populations at a single-cell level (Seidemann et al., 2016; Tian et al., 2012). However, as rAAV transduction ensues, Ca^{2+} fluorescence signal strength is rarely adequate to image cortical activity earlier than two weeks post-injection (Attinger et al., 2017; Iacaruso et al., 2017; Pakan et al., 2016; Zmarz and Keller, 2016). Based on our anatomical findings we predicted that doxorubicin treatment should reduce this delay period, and thus tracked transgene expression *in vivo* with two-photon imaging in mice.

For this experiment we used rAAV9 encoding GCaMP6s indicator under the control of the synapsin promoter (rAAV9-hSyn-GCaMP6s; titer: 2×10^{12} vg/ml, 1 μl per injection). This vector was stereotaxically injected into the mouse primary visual cortex (V1) in combination with, or without doxorubicin (10 μg/ml). As shown by **Figure 6** for a large window of brain surface, the fluorescence signal in doxorubicin-treated sites was evident at the sixth day after injection, at which time point it was undetectable in the control (**Figure 6A**). Quantitative measurements of fluorescence signal revealed that doxorubicin more than doubled the rate of expression of GCaMP6s, reaching a plateau at 30 days, whereas the control mice achieved 50% of this level of expression much later, at around 60 days (n = 5 per group, **Figure 6B**). We chose the sixth day after the injection of rAAV9 plus doxorubicin to perform *in vivo* two-photon Ca^{2+} imaging. When examined with two-photon microscopy, the morphology of cell bodies was clearly observable under doxorubicin-treated conditions, unlike the control (**Figure 6C** and **6D**). Furthermore, using drifting sine-wave gratings as visual stimuli, robust direction-selective responses of mouse V1 neurons could be recorded after doxorubicin-treatment, but not in the control. Note that the neural activities in untreated mice could not be obtained until two weeks later. To test whether doxorubicin treatment had any impact on neuronal functions, we compared the response strength ($\Delta F/F$) and orientation selectivity of mouse V1 neurons in cases with or without and doxorubicin-treatment, respectively at 15 versus 30 days post injection. We found that V1 neurons showed little significant difference between the two conditions in their response strength (Wilcoxon rank-sum test, $p = 0.25$; median of control group 0.43, median of doxorubicin group 0.42) and orientation selectivity (Wilcoxon rank-sum test, $p = 0.06$; median of control group 0.127**,** median of doxorubicin group 0.116**; Figure S4**). These results imply that the functional response properties of neurons were not affected by doxorubicin treatment.

Together these results demonstrated that doxorubicin not only accelerates transgene expression, enabling earlier commencement *in vivo* two-photon imaging, but also has little effect on cortical neuron functionality in the conditions we tested.

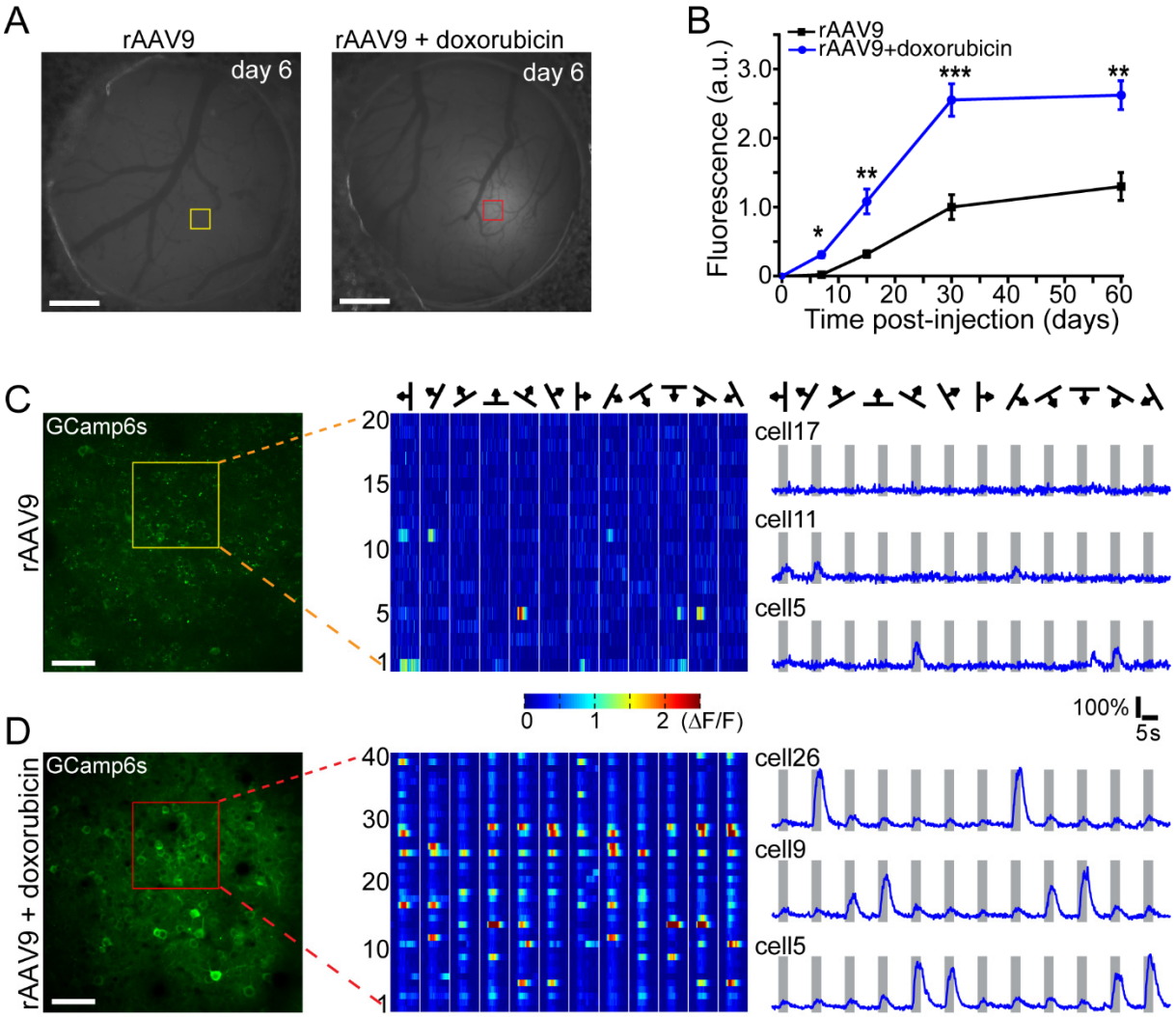

Figure 6. Doxorubicin Induces a Rapid Onset of Transgene Expression for *In Vivo* Study of Neural Function (**A**) Representative fluorescence images of mouse V1 six days after vector administration with or without doxorubicin. rAAV9-hSyn-GCaMP6s vector (titer: 2×10^{12} vg/ml, 1 µl per injection) was injected with 10 µg/ml doxorubicin. Scale bar, 1 mm. (**B**) *In vivo* tracking of GCaMP6s expression after injection of rAAV9-hSyn-GCaMP6s vector alone and with doxorubicin (10 µg/ml) in mouse visual cortex over 0-60 days. N = 5 mice per group, mean ± s.e.m. Wilcoxon rank-sum test, *$p < 0.05$. **$p < 0.01$. ***$p < 0.001$. (**C,D**) *In vivo* two-photon image of Ca^{2+} fluorescence assessed after only 6 days of expression at a focal plane of injection sites (~120 µm below cortical surface, as indicated in **A**). Mean fluorescence changes (ΔF/F) of sampled cells (boxed in **C-D**) evoked by drifting sine-wave grating stimuli. Scale bar, 50 µm.

Doxorubicin Enables Efficient Retrograde Tracing of Connections in Macaque Cortex and Thalamus

Apart from enabling many novel methodologies, viral technology has also seen rapid uptake by classical neuroanatomy (Nassi et al., 2015). rAAV vectors can undergo both anterograde and retrograde axonal transport, contingent upon the varying efficacy of different serotypes for selective uptake by proximal dendrites or axonal terminals (Castle et al., 2014; Green et al., 2016; Yazdan-Shahmorad et al., 2018). Tracing the functional organization of trans-areal circuit connectivity by means of viral methods relies on high levels of transgene expression, and a novel variant, rAAV-retro, has recently been developed for the express purpose of maximizing retrograde access to projection

neurons (Diester et al., 2011; Tervo et al., 2016). Given the long known finding that doxorubicin, also undergoes retrograde transport from uptake at axonal terminals (Bigotte and Olsson, 1982; Kato et al., 1988; Koda and Van der Kooy, 1983), we considered that doxorubicin have good prospects for remote circuit-selective enhancement of rAAV transduction and therefore could be used for neural circuit interrogation.

We conducted these experiments in the primate, in view of the growing importance of systematic, quantified connectional databases (connectomics) in understanding human brain function (Markov et al., 2014; Oligschlager et al., 2019; Wang and Kennedy, 2016), at the same time assessing the efficacy of rAAV-retro in this species. The vector (rAAV2-retro-CAG-tdTomato; 4×10^{13} vg/ml, 1μl) was infused bilaterally into area V1, either in combination with doxorubicin (10 μg/ml) (right hemisphere) or vector alone as a control (left hemisphere) (**Figure 7A**). At six weeks after injection, we examined tdTomato expression amongst retrogradely labeled cells in the lateral geniculate nucleus (LGN), as well as cortical areas including V2, V4 and MT that send long-range projections to V1 (**Figure 7A**). Before examination, we first confirmed good rAAV2-retro transduction across all layers at the injection site of V1 (**Figure 7B**). In the LGN, the main subcortical source of input to V1, we observed many neurons labeled with tdTomato fluorescent protein (**Figure 7C**). Consistent with previous reports based on tracer dyes (Angelucci and Sainsbury, 2006; Kennedy and Bullier, 1985), the cell bodies of labeled neurons were concentrated in a narrow strip across the six-layer structure of LGN, surrounded by nerve fibers. Compared with the control side, the number of cells labeled with tdTomato on the right side of LGN was far greater, and tdTomato expression was stronger in both neuron cell bodies and fibers (**Figure 7C**, **7D** and **Figure S5A**). Amongst prestriate cortical areas, we found large numbers of tdTomato-labeled cells in V2, concentrated in a retinotopically matching subregion close to the injection site in V1(**Figure 7E**), consistent with previous studies (Perkel et al., 1986; Rockland and Pandya, 1979; Rockland and Virga, 1989; Weller and Kaas, 1983). Again, compared with the left control side, the number of tdTomato-positive cells in the right V2 was greater, and the fluorescent signal was stronger across serial sections (**Figure 7F** and **S5B**), so confirming the enhancement effect of doxorubicin to be mediated via retrograde transport in corticocortical as well as thalamocortical projections. This enhancement was equally clear in longer-range projections - we detected many tdTomato-positive neurons in V4, MT and other visual cortices in the right hemisphere, with little or even no tdTomato signal in the left control side; in this respect, performance of rAAV-retro unaided by doxorubicin was notably poor in comparison to conventional retrograde tracers (**Figure 7G-I** and **S5C-D**). These results confirmed that doxorubicin can induce a circuit-selective enhancement of rAAV transduction via axonal retrograde transport, and could thus be a useful supplementary tool for analysis of neural circuits in large mammals like the macaque.

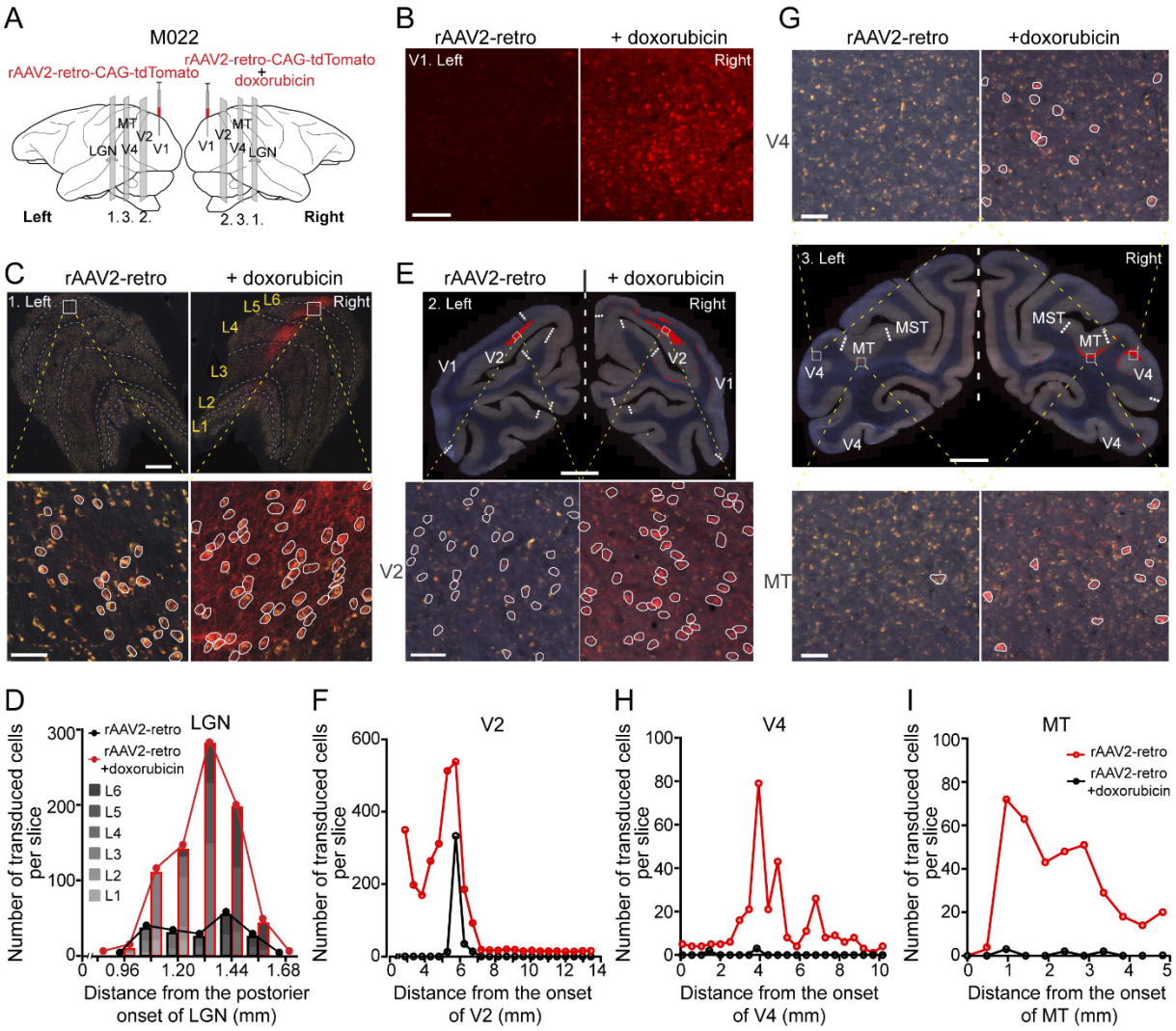

Figure 7. Enhancement of rAAV Transduction via Retrograde Axonal Transport in Macaque Thalamo- and Cortico-Cortical Circuits

(**A**) Schematic showing injections and quantified sources of afferents to V1, including LGN (panel 1), V2 (panel 2), V4 and MT (panel 3). rAAV2-retro-CAG-tdTomato vector (titer: 4×10^{13} vg/ml, 1 μl per injection), vector alone or coupled with doxorubicin (10 μg/ml), was injected at symmetrical locations in the left and right hemispheres, respectively, of monkey V1. Transduced neurons were assessed in 40μm coronal sections after six weeks of expression. (**B**) Representative images of neuronal transduction at the injection site of rAAV2-retro alone, or combined with doxorubicin. Scale bar, 100 μm. (**C**) Representative images of LGN from hemispheres with rAAV2-retro alone or combined with doxorubicin. Transduced neurons from ROI (boxed in the upper panel) were marked by white circles. Scale bar, 500 μm (upper), 50 μm (lower). (**D**) Comparison of retrograde transport efficiency for LGN. The transduced cells were counted across six layers in sample sections taken every 120 μm sequentially across LGN. (**E**) Representative images of V2 from hemispheres with rAAV2-retro alone or combined with doxorubicin. Upper panel: whole coronal image (transduced cells are marked with red dots); Lower panel: transduced neurons from ROI (boxed in the upper panel) are marked by white circles. Scale bar, 500 μm (upper), 50 μm (lower). (**F**) Comparison of retrograde transport efficiency for V2. (**G**) Representative images of V4 and MT from hemispheres with rAAV2-retro alone or coupled with doxorubicin. Middle panel: whole coronal image of macaque brain (transduced cells are marked with red dots); Top and bottom panels: transduced neurons from ROIs of V4 and MT are marked by white circles. Scale bar, 500 μm (middle), 50 μm (top and bottom). (**H-I**) Comparison of retrograde transport efficiency for V4 and MT. In **F**,**H** and **I,** transduced cells were counted in regions of V2, V4 and MT within sample sections taken every 480 um across the brain from posterior to anterior.

DISCUSSION

With recent advances in vector engineering, rAAVs have met with great success as carriers for *in vivo* gene transfer (Wang et al., 2019). Clinical trials of rAAV-based gene therapy have demonstrated clear therapeutic efficacy (Chien et al., 2017; Christine et al., 2019; Mendell et al., 2017; Mittermeyer et al., 2012; Tardieu et al., 2014). rAAV has also become a powerful tool for cell type-specific gene modulation in many fields of basic neuroscience (Betley and Sternson, 2011). However, it is also recognized that rAAV still has some shortfalls, which include insufficient transduction in targeted tissues and tardiness of gene expression after transduction (Wang et al., 2019). Therefore, more efficient strategies for rapid-onset and high-level transgene expression at lower doses are much to be desired for *in vivo* rAAV transduction. Here we outline how the clinical pharmacological agent ***doxorubicin*** might be exploited to enhance the efficiency of transgene expression in a range of basic and therapeutic research applications across various combinations of rAAV serotype and experimental species.

Mechanism and Time Course of Doxorubicin Action

After infection of the host cell the rAAV genome (constituted of single-stranded DNA) has to undergo several processes before transgene expression can occur (Balakrishnan and Jayandharan, 2014), amongst which intracellular trafficking and second-strand DNA synthesis are two rate-limiting steps (Ferrari et al., 1996; Fisher et al., 1996). The action of doxorubicin – an inhibitor of topoisomerase II and DNA synthesis (Tacar et al., 2013) – to facilitate this process is therefore paradoxical. A clue may exist in the long-known finding that agents causing DNA damage, including ionizing radiation, have the same general capability as topoisomerase-inhibitors to enhance the efficiency of rAAV transduction (Alexander et al., 1994; Kanazawa et al., 2001; Nicolson et al., 2016; Prasad et al., 2007; Russell et al., 1995). This capability may, perhaps, be an indirect consequence of the cellular reaction to DNA damage: the 'decoy' thesis posits that rAAV replication is normally restrained by DNA-damage response proteins, which become preferentially engaged in the work of DNA repair (Choi et al., 2006; Nicolson et al., 2016). Furthermore, doxorubicin may also promote viral nuclear entry through modulation of proteasome function (Yan et al., 2004). We embarked on a series of experiments testing the effect of doxorubicin upon transgene expression mediated by rAAV8 in cat cortex. As anticipated, we observed a remarkable enhancement of transduction following doxorubicin treatment (**Figure 1**), consistent with previous studies utilizing rAAV2 (Zhang et al., 2012; Zhang et al., 2009). Furthermore, doxorubicin enhanced the rapidity of cellular transduction by rAAV: we found that the time required for transgene expression to reach detection level decreased from around 7 days to 3 days, with a sustained increase of expression thereafter (**Figures 2** and **6**). In short, we infer doxorubicin to have an intracellular action that favors the accrual of stable, dual-stranded AAV DNA as an 'episome'

(Balakrishnan and Jayandharan, 2014) (i.e. separate from the host cell chromosome) within the cell nucleus. This augments expression of the viral DNA, subject to any regulatory elements included within the vector genome. Subsequent investigation served to confirm the generality of this accelerated transduction achievable with doxorubicin.

The Generality of Doxorubicin-Mediated Transduction Enhancement

AAV has multiple serotypes with varying characteristics and new AAV variants with superior efficacy continue to be developed through vector engineering approaches, that essentially seek to 'fine-tune' the binding properties of the capsid to cell surface receptors (Srivastava, 2016; Wang et al., 2019). To examine the plurality of doxorubicin enhancement we extended our study of rAAV8 to other AAV serotypes such as rAAV2, rAAV9 and rAAV-PhP.eB. AAV2, as the first serotype to be sequenced and cloned, has seen the broadest research use, although it is less effective for cortical transduction (Watakabe et al., 2015). AAV-PhP.eB is a variant of AAV9 obtained recently by directed evolution for improved capability to bypass the blood-brain barrier (Chan et al., 2017; Deverman et al., 2016). Testing these vectors of different serotypes, we found that rAAV-PhP.eB roughly matched the performance of rAAV8 for transgene expression in cat cortex, and confirmed less expression on the part of rAAV2. However all three showed marked enhancement by doxorubicin, of roughly comparable proportionate magnitude, suggesting a serotype-general effect of doxorubicin upon rAAV transduction. For further substantiation, we extended our investigation across species, and found that doxorubicin achieved similar levels of enhancement for transduction by rAAV-PhP.eB in the cortex of macaque monkey, and of the mouse, as it did in the cat (**Figure 5**).

In addition to species- and serotype-generality, we can also consider if doxorubicin perturbs specificity of transgene expression across different cell types, either by interfering with the cell tropism of rAAV vectors, or with cell-specific regulation of transcription. Our experiments allowed us to compare the action of doxorubicin in conjunction with rAAV vectors carrying either the neuron-specific hSyn or the ubiquitous CAG promoter. Studies on mouse and marmoset concur that rAAV vectors carrying the hSyn promoter show a proclivity for transgene expression in inhibitory neurons and larger pyramidal neurons (Nathanson et al., 2009; Watakabe et al., 2015). We also found that layer 4, characterized by smaller pyramids, showed the lowest percentage of transgene expressing neurons when treated with rAAV8 vectors carrying hSyn promoter, and consequently the greatest proportional increase with doxorubicin (the effect in other layers being limited by increasing saturation of expression). Most importantly, with hSyn promoter, transgene expression with doxorubicin remained restricted to neurons (as indicated by 100% co-expression of the NeuN marker, **Figure 1D**), giving no evidence of doxorubicin interference with cell type specificity governed by promoters. With CAG promoter we observed, as expected, additional expression of transgene by

astrocytes; doxorubicin treatment induced a similar enhancement in both neurons and astrocytes, but did not alter the negative status of microglia transduction (**Figure S1**). We therefore obtained no indication that doxorubicin can alter the fundamental tropism of an rAAV vector.

Given what is known of the molecular biology of doxorubicin action (reviewed above) the ensemble of our findings suggests the analogy to chemical catalysis: doxorubicin enhances the speed and level of transgene expression, but does not affect the tropism for cell type (as governed by the capsid), nor alter the specificity of cellular expression (as governed by regulators of transcription). Hence, in principle, doxorubicin enhancement should prove a valuable strategy for optimizing rAAV transduction in many fields of research practice.

Absence of Neurotoxicity at an Effective Clinical Dosage

Cytotoxicity is the foremost concern prohibiting exogenous agents from *in vivo* application to promote rAAV transduction (Nicolson et al., 2016; Prasad et al., 2007; Russell et al., 1995; Yan et al., 2004). As a chemotherapeutic drug, doxorubicin takes effect in cancer treatment by inhibiting cell proliferation and inducing apoptosis (Tacar et al., 2013). For non-dividing cells, such as neurons, there is less expectation of significant cytotoxicity (although cardiac tissues are known to be affected in high-dose schedules) (Maini et al., 1997). Direct delivery into the brain, rather than intravenous administration, restricts doxorubicin uptake to cells within the local injection area. Our *in vivo* dose-finding study found that 1 μl of injectate significantly enhances rAAV transduction at a doxorubicin concentration of 1~10 μg/ml (or 1.72~17.2 μM) (**Figure 3**). Injecting 1μl into the cerebral cortex of cats and mice at a concentration of 10 μg/ml, we detected little cytotoxicity: infected neurons maintained healthy morphology and function upon histological examination (**Figure 1C** and **3**) and *in vivo* imaging (**Figure 6** and **Figure S4**) at 7~30 days post-injection. Further examinations revealed no apoptosis at the site of injection (**Figure 4A**), nor any inflammatory response (**Figure 4B**). At the behavioral level, our trial animals (mice) also presented normal locomotor activity (**Figure S2**). This non-neurotoxic concentration of doxorubicin (1.72~17.2 μM) is within the 10-24 μM range of peak bloodstream plasma concentrations measured in humans following intravenous doxorubicin administration (50 mg/m^2) in clinical cancer chemotherapy (Mross et al., 1988). Furthermore, following direct injections into the cortex, or other brain sites, the concentration will fall several-fold upon diffusion through neural tissues. Overall, these results confirm the feasibility of the use of doxorubicin to catalyze rAAV transduction at a dosage effectively matching clinical practice.

How Would Doxorubicin-Enhanced Transduction Work in Practice?

Our standard approach mimics many research applications in seeking to transduce neurons in a single local patch of cortex. This includes induction of GCaMP6 for two-photon imaging of neural activity, as recently attained in alert primate (Ju et al., 2018; Li et al., 2017), or a marker like GFP to

reveal efferent axon terminals (Oh et al., 2014), or an effector such as ChR2 to allow optical stimulation of axon activity at remote locations (Yang et al., 2013; Zhang et al., 2014). Though there have been many such successful applications of these methods, enhanced levels of transduction can only be to the advantage of the experimental goals. Furthermore, we also demonstrated remote, non-local enhancement via retrograde transport using rAAV2-retro, thus expanding potential doxorubicin applications to include neural circuit interrogation and delivery of effectors (such as GCaMP6) to specific subsets of projection neurons (Tervo et al., 2016). More problematic are applications that seek to modulate the activity of extensive cortical regions, such as an entire functional area, requiring multiple viral injections (Eldridge et al., 2016). Here the application of doxorubicin could make a strategic difference to the practicality and outcome of a research project, raising the ceiling for what is considered feasible.

Similar considerations arise for subcortical nuclei of large volume, for instance the putamen. This is particularly the case where the goal is to transduce as much tissue as possible, typically for therapeutic research relating to Parkinsons disease. In a technical advance over previous work, the most recently completed clinical trial (Christine et al., 2019) employed convection-enhanced delivery (Mehta et al., 2017) (a pressure-aided form of microperfusion previously trialed in nonhuman primate (Johnston et al., 2009)) infusing upto 900µl to attain 20-40% coverage of the total putaminal volume. Whilst the assessment of the therapeutic benefits of this treatment was positive, an enhancement of transduction efficiency – as achieved by co-administration of doxorubicin – should give additional benefit. At the concentration we found to be effective (1~10 ug/ml), ~1ml of infusate delivered bilaterally would amount to 2~20ug of doxorubicin, again dramatically less than a typical clinical dose (~100mg). In common with other clinical trials (Christine et al., 2019), this study made use of an AAV2 vector, whereas research in nonhuman primates has found almost all AAV serotypes, and particularly AAV5, to be superior to AAV2 for striatal transduction (Dodiya et al., 2010; Markakis et al., 2010). As reasoned above, we infer that doxorubicin should be equally effective in conjunction with any AAV serotype.

Comparable trials in primate models of Parkinson's disease confirm that the principal cell type of the striatum, the medium spiny neuron (MSN) was transformed by rAAV transgenes (coding for dopamine synthesis enzymes) to acquire a dopaminergic function (Sehara et al., 2017). Whilst no equivalent GABAergic projection neuron exists in the cortex, our evidence for general doxorubicin 'catalysis' of AAV transduction, coupled to previous study of rat striatum (Zhang et al., 2009), imply that doxorubicin would facilitate MSN transduction in human subjects. And, whilst the natural tropism of AAV is relatively broad, effective transduction can be narrowed to neural classes specified by regulatory elements packaged into the vector genome. For instance use of the dlx enhancer in rAAV restricts expression of transgenes to GABAergic interneurons in all tested species (Dimidschstein et

al., 2016); hence doxorubicin should act to selectively enhance transduction of interneurons if co-administered with rAAV carrying interneuron-specific enhancers.

Finally, in standard clinical practice, doxorubicin is administered by intravenous injection, and that route might prove advantageous for enhancing transduction across broad cortical territories, if it were capable of passing the blood-brain barrier (BBB). In view of the potential for doxorubicin as an agent in neuroglioma therapy, the latter is the subject of active research in animal models (Alli et al., 2018) and a first 'proof of concept' clinical trial (Mainprize et al., 2019). If techniques enabling doxorubicin to pass the BBB can be perfected, it would open the door to intravenous co-administration with strains of AAV with the natural capacity to pass the BBB and achieve general CNS transduction (Samaranch et al., 2012; Yang et al., 2014). This route faces the challenge of natural immunity (Colella et al., 2018; Samaranch et al., 2012), and requires substantially larger amounts of virus; nevertheless, several AAV variants, including one that we tested in macaques (rAAV-PHP.eB) have been derived specifically to enhance this capability (Chan et al., 2017). Intravenous co-administration might be applied to address acute conditions such as stroke, exploiting the speedier transgenic expression achievable with doxorubicin. Past gene therapy studies for animal models of stroke have demonstrated benefits from a variety of transgenes, typically administered by direct injection of rAAV, but *prior* to the experimental induction of ischemia (Harvey et al., 2011; Lu et al., 2012; Sehara et al., 2018). The effective doubling of the rate of transduction achievable with doxorubicin could provide the key to unlock the clinical potential of transgenic therapy in such emergency contingencies.

In summary, our study has demonstrated that application of doxorubicin facilitates rAAV transduction in rodent, carnivore and primate cerebral cortex. This enhancement of doxorubicin on rAAV takes effect at doses well below tolerance without detectable cytotoxicity to neural tissues. Our findings suggest a feasible strategy synergistic with ongoing vector system engineering to optimize rAAV transduction, so to attain more rapid and more efficient transgene expression *in vivo*.

ACKNOWLEDGMENTS

This work was supported by the Strategic Priority Research Program of Chinese Academy of Sciences, Grant No. XDB 01060200; the Shanghai Municipal Science and Technology Major Project, Grant No. 2018SHZDZX05; National Natural Science Foundation of China Grant No. 31861143032.

AUTHOR CONTRIBUTIONS

W.W. designed research; HL.G., NN.Y., ZM.S., C.T., performed research; S.S., LL.Q, YL.L, I.M.A., SH.Z, JH.W., and G.Y. contributed analytic tools; HL.G. analyzed data; HL.G., S.S., and W.W. wrote the paper.

DECLARATION OF INTERESTS

The authors declare no competing interests.

STAR★METHODS

KEY RESOURCES TABLE

REAGANT or RESOURCE	SOURCE	IDENTIFIER
Bacterial and Virus Strains		
rAAV8-hSyn-EGFP	ION Gene Editing Core Facility	N/A
rAAV8-CAG-EGFP	ION Gene Editing Core Facility	N/A
rAAV-PHP.eB-CAG-EGFP	ION Gene Editing Core Facility	N/A
rAAV2-CAG-EGFP	Taitool Bioscience (Shanghai)	N/A
rAAV9-hSyn-GCaMP6s	Taitool Bioscience (Shanghai)	Cat# S0528
rAAV2-retro-CAG-tdTomato	Got from Dr. Yuejun Chen' Lab	N/A
Chemicals, Peptides, and Recombinant Proteins		
Doxorubicin hydrochloride	Sigma-Aldrich	Cat# D1515-10mg
Antibodies		
Mouse anti-NeuN	Millipore	Cat# MAB377; RRID:AB_2298772
Rabbit anti-GFAP	Invitrogen	Cat# MA119170; RRID:AB_1074604
Rabbit anti-Iba1	Wako	Cat# 01919741; RRID:AB_839504
goat anti-mouse antibody, Alexa Fluor 555	Life Technologies	Cat# A21424; RRID:AB_141780
goat anti-rabbit antibody, Alexa Fluor 555	Life Technologies	Cat# A32732; RRID:AB_2633281
Critical Commercial Assays		
One Step TUNEL Apoptosis Assay Kit	Beyotime technology	Cat# C1089
Experimental Models: Organisms/Strains		
Mouse: C57BL/6	SLAC laboratory	N/A
Cat	ION animal facility	N/A
Rhesus Macaque (Macaca mulatta)	ION Primate Center, Shanghai	N/A
Software and Algorithms		
ImageJ	NIH	RRID:SCR_003070
GraphPad Prism 7	GraphPad	RRID:SCR_002798
MATLAB	MathWorks	RRID:SCR_001622
Other		
E80i microscopy	Nikon	N/A
VS120 virtual slide microscope	Olympus	N/A
TiE-A1plus Laser Scanning Confocal microscope	Nikon	N/A
Two-photon microscope	Thorlabs	N/A
Axio Scan. Z1	ZEISS	N/A
Ti-Sa laser	Spectra-physics	N/A

RESOURCE AVAILABILITY

Lead Contact

Information and requests for resources should be addressed to the Lead Contact, Dr. Wei Wang

Materials Availability

All unique resources generated in this study are available upon reasonable request to lead contact.

Data and Code Availability

No unique code was generated in this study.

EXPERIMENTAL MODEL AND SUBJECT DETAILS

Experimental subjects were adult cats, C57BL/6 mice and rhesus macaques (Macaca mulatta). All experimental procedures were approved by the Animal Care and Use Committee of the Institute of Neuroscience, Chinese Academy of Sciences, and were carried out under the instruction of the National Institutes of Health Guide for the Care and Use of Laboratory Animals.

Mice

Thirty-three Male C57BL/6 mice of 8 weeks age were purchased from Slac Laboratory Animals (Shanghai). All mice were raised under constant temperature, humidity and automatic light cycles (12 hours light/dark). Mice were used for in vivo two-photon calcium imaging experiment, behavior test and cross-species examination.

Cats

Thirty adult cats of both sexes (age: 1-3 years; weight: 2.5-3.5 kg) were obtained from the animal facility of the Institute of Neuroscience. All cats were raised under constant temperature, humidity and automatic light cycles (12 hours light/dark).

Macaque monkeys

Three macaque monkeys (two males and one female, 6-8 years old, weight: 6.0-9.0 kg) were used in this study, two for cross-species examination and another for neural circuit interrogation. All animals were raised under constant temperature, humidity and automatic light cycles.

METHOD DETAILS

Virus and drug preparation

The rAAV vectors and sources were the following: rAAV8-hSyn-EGFP, rAAV8-CAG-EGFP, rAAV-PHP.eB-CAG-EGFP (ION Gene Editing Core Facility), rAAV2-CAG-EGFP, rAAV9-hSyn-GCaMP6s (Taitool Bioscience, Shanghai) and rAAV2-retro-CAG-tdTomato (obtained from Dr. Yuejun Chen). Doxorubicin (doxorubicin hydrochloride) was purchased from Sigma-Aldrich and dissolved in sterile phosphate buffered saline (PBS). For injection, viral solutions were diluted and prepared with PBS just before experiment, which consisted of rAAV and 10 μg/ml doxorubicin (or as indicated). As a control, viral solutions contained only rAAV in PBS.

Surgery and stereotaxic injection

For virus injection, adult cats were anaesthetized with ketamine hydrochloride (25 mg/kg) and then positioned in a custom-made stereotaxic apparatus with anesthesia maintained by isoflurane (1.5-2.0%). Small skull holes (~1 mm^2) were made in both hemispheres at Horsley-Clarke coordinates A5-P7, L2-L3 (Figure 1A). Dura incisions were made for introduction of glass pipettes (tip diameter of 40-50 μm) into the cerebral cortex (a depth of ~1000 μm from cortical surface). Injections of viral solutions were performed through glass micropipettes at a rate of 90

nL/min by a microinjector (QSI). After injection, micropipettes were kept in place for 10 minutes prior to withdrawal. Pulse oxygen saturation, electrocardiograph, end-tidal carbon dioxide and core body temperature were monitored throughout the surgical procedure. After surgery, animals recovered from the anesthetic and cefotaxime sodium (80 mg/kg) was applied through intraperitoneal injection twice a day in the following seven days.

To examine the effect of doxorubicin on rAAV-mediated neuronal transduction, rAAV8-hSyn-EGFP (titer: 1×10^{12} vg/ml) was injected into the right and left hemisphere of three cats with or without doxorubicin (10 μg/ml) at a volume of 1000 nl for each injection. Histological examination was carried out at 30 days post-injection.

To determine the optimal dosage of doxorubicin for neurological administration, different concentrations of doxorubicin (0.1-100 μg/ml) were injected with rAAV8-hSyn-EGFP (titer: 1×10^{12} vg/ml) into the visual cortex of six cats at a volume of 1000 nl for each injection, with injections of rAAV8-hSyn-EGFP only as control. Histological examination was carried out at 7 days post-injection.

To assess the impact of doxorubicin on the kinetics of rAAV transduction, rAAV8-hSyn-EGFP (titer: 1×10^{12} vg/ml) coupled with doxorubicin (10 μg/ml) or PBS was administered into the visual cortex of twelve cats at a volume of 1000 nl for each injection, three cats per group. Histological examination was carried out at 3, 7, 15 and 30 days post-injection.

To determine whether doxorubicin exerts a general agonist effect upon rAAV transduction, rAAV-CAG-EGFP vectors (rAAV8, rAAV-PHP.eB and rAAV2, titer: 5×10^{11} vg/ml) were injected into the visual cortex of five cats with or without doxorubicin (10 μg/ml) at a volume of 1000 nl for each injection. Histological examination was carried out at 7 days post-injection.

To assess the cytotoxic effects of doxorubicin upon neural tissues, five cats were injected with PBS, doxorubicin (10 μg/ml), and rAAV8 vector (rAAV8-hSyn/CAG-EGFP, titer: $0.5\sim1 \times 10^{12}$ vg/ml) with or without 10 μg/ml doxorubicin at a volume of 1000 nl for each injection. Seven days following injection, animals were prepared for TUNEL assay and inflammatory examination.

For virus injection in mouse, animals were anaesthetized by 1.5~2.0% isoflurane or intraperitoneal injection of pentobarbital sodium (80 mg/kg) and mounted in a stereotaxic apparatus with body temperature kept at 37 °C. In the cross-species examination, rAAV-PHP.eB-CAG-EGFP (titer: 5×10^{11} vg/ml, 1μl) alone or coupled with 10 μg/ml doxorubicin was injected into the primary visual cortex (V1) of four mice (stereotaxic coordinates: 2.1 mm posterior to bregma, 1.8 mm lateral to midline, 0.6 mm vertical from cortical surface) through a skull hole at a rate of 90 nl/min with a glass pipette (tip diameter of 20-30 μm). In the open field test, rAAV8-hSyn-EGFP (titer: 1×10^{12} vg/ml, 1μl) alone or coupled with 10 μg/ml doxorubicin was injected into the primary motor cortex of right hemisphere of nineteen mice (stereotaxic coordinates: 0.5 mm anterior from bregma, 1.5 mm lateral from the midline, 0.6 mm vertical from cortical surface). For two-photon calcium imaging, a circular craniotomy (~3 mm diameter) was made to expose the primary visual cortex. rAAV9-hSyn-GCaMP6s (2×10^{12} vg/ml, 1μl) coupled with doxorubicin (10 μg/ml) or vector alone was injected into area V1 of ten mice, at a depth of 0.6 mm beneath cortical surface. After injection, the dura was removed and a chronic window was made with custom-made double-layered coverslip covering the cortex. For repeated imaging, a custom-made titanium headplate was implanted with dental acrylic. After surgery, antibiotics were administered by intramuscular injection and animals were given about 7 days (or as indicated) for recovery before experiment.

The three adult macaque monkeys used in this study underwent the same preparatory procedure. Following induction by ketamine hydrochloride (15 mg/kg), deep anesthesia was maintained with isoflurane (1.5-2.0%) whilst the head of animal was mounted in the stereotaxic apparatus and prepared for craniotomy, durotomy and

viral injection. In the cross-species examination, rAAV-PHP.eB-CAG-EGFP vectors (titer: 1×10^{12} vg/ml) were injected into the motor cortex (at a depth of 1500 μm) through glass pipettes (tip diameter of 40-60 μm) with or without doxorubicin (10 μg/ml) at a volume of 2000 nL for each injection. For neural circuit interrogation, rAAV2-retro-CAG-tdTomato (titer: 4×10^{13} vg/ml, 1μl per injection) was injected into the left and right hemisphere of monkey V1 symmetrically, vector alone or coupled with doxorubicin (10 μg/ml). Throughout the surgical procedure, pulse oxygen saturation, electrocardiograph, end-tidal carbon dioxide and core body temperature (37~38 °C) were monitored. After injection, micropipettes were kept in place for 10 minutes prior to withdrawal and animals were carefully maintained for recovery. Histological examination was carried out at 7 days or 42 days post-injection.

Histology and image acquisition

Animals were deeply anaesthetized with sodium pentobarbital, followed by transcardial perfusion of 0.9% NaCl and 4% paraformaldehyde (wt/vol) in PBS. Brains were removed and post-fixed with 4% paraformaldehyde in PBS for 12~48 hours, and then dehydrated with 30% sucrose (wt/vol) for about 1~5 days. For each brain every injection site was identified and marked under a fluorescence stereoscope (Stereo Discovery V20, Zeiss). Fixed brains were cut into 50 μm thick coronal sections on a freezing microtome. Representative sections from each injection site showing the largest amount of fluorescence were identified and selected for subsequent assay. For immunohistochemistry, sections were first rehydrated with PBS and preincubated with blocking solution (PBS with 1% bovine serum albumin and 0.5% Trixon-100) before incubation with primary antibodies at 4 °C overnight. Antibodies against neuronal or glial marker proteins were used as follows: neuron-specific nuclear protein (mouse anti-NeuN; 1:500), glial fibrillary acidic protein (rabbit anti-GFAP; 1:500) and ionized calcium binding adaptor molecule (rabbit anti-Iba1, 1:500). After rinsing with PBS, sections were incubated with secondary antibody (goat anti-mouse antibody, 1:1000; goat anti-rabbit antibody, 1:1000) for 2 hours at room temperature. DAPI was added to a final concentration of 1 μg/ml for staining cell nuclei.

Large field images of representative sections from each injection were first examined with Nikon E80i or Olympus VS120 fluorescence microscope using a 10x objective. Confocal fluorescence images were then acquired by Nikon TiE-A1plus confocal laser scanning microscope using a 20x/0.75NA objective. For GFP intensity quantification, the background fluorescence of images was obtained from a remote reference region site and subtracted. GFP signal was identified and calculated from pixels with fluorescence values exceeding the mean background by three standard deviations. To evaluate the effect of doxorubicin, a region of interest (ROI) with 500 x 1300 μm size at the core of each injection was selected for calculation of GFP intensity. For cell number counting, stack images of 10-μm depth were acquired on Nikon TiE-A1plus confocal laser scanning microscope using a 40x/1.3 NA objective. Cells were identified with antibodies identifying cell-type specific marker, NeuN for total neurons, GFAP for astroglia, and Iba1 for microglia. Cell counting was performed manually or automatically using ImageJ (NIH).

For neural circuit interrogation in macaque monkey, the whole brain was dehydrated with 20% glycerol in PBS, and cut into 40-μm-thick coronal sections symmetrically. Representative sections of LGN, V2, V4, MT and V1-injection sites showing the largest amount of transduced cells were identified and selected for subsequent analysis (Figure 7). Large field images were obtained with ZEISS Axio Scan Z1 fluorescence microscope using a 10x objective and tdTomato-positive cells were counted manually. For LGN, confocal images of 5 μm thickness were taken and tdTomato-positive cells were identified and counted manually. Pictures were stitched together with Adobe Illustrator software.

Two-photon calcium imaging

Mice were anaesthetized by 0.7~1.0% isoflurane via respiration and fixed with the implanted headplate. Body temperature was maintained at about 37°C with a heating pad, and animal state was monitored using an infrared camera. Images were acquired within an ROI (1024 x 1024 pixels) with a commercial two-photon microscope (Thorlabs) which was controlled by ThorImage software, via a 16× objective (NA = 0.8, Nikon). GCaMP6s-based Ca^{2+} signal was excited with 910-nm wavelength that generated via a mode-locked Ti:sapphire laser (Mai Tai DeepSee, Spectra physics), and collected with filter 525/50. Visual stimuli were generated with the Psychtoolbox for MATLAB and presented monocularly on a 17-inch LCD monitor (Lenove) at a distance of 15 cm in front of the animal. Sinusoidal gratings (contrast = 1; spatial frequency = 0.05 cycle/degree; temporal frequency = 2 cycle/second) were displayed for 3 seconds and drifted at eight directions (0°, 45°, 90°, 135°, 180°, 225°, 270°, 315°) randomly, five repeats per condition. For each condition, images were captured at a frame rate of 7.8 Hz over a period of 8 seconds, including 1 second before stimuli onset. Before experiment, baseline fluorescence was collected for 200 frames without visual stimuli and treated as an indicator of GCaMP6s expression.

Images obtained in our experiment were analyzed with ImageJ (National Institutes of Health) and Matlab (Mathworks). For correcting lateral motion in the imaging data, a rigid-body transformation based frame-by-frame alignment was applied by using Turboreg plugin (ImageJ software). Cells were identified on the basis of cross-trial variability calculation and manually modified by empirically handed labeling according to the size, shape, and brightness. Fluorescence changes with time of individual cells were extracted by averaging pixel intensity values within each cell in each frame. Fluorescence intensity change (ΔF) evoked by each stimulus (stimulus duration, 3s) were normalized by the pre-stimulus baseline fluorescence (F, 1 s). For each stimulus, the mean change in fluorescence (ΔF/F) was calculated by averaging responses to all trials for each stimulus condition. Cells showing significant differences in the fluorescence intensity signals observed during baseline vs. stimulus-presentation periods ($P<0.05$, ANOVA) were defined as "responsive cells". The response strength was determined as the maximal (ΔF/F) across all the stimulus conditions. The orientation selectivity index (OSI) was defined as (1-Var(θ)), where Var(θ) is the circular variance of the responses to the tested directions.

TUNEL assay

The TUNEL assay was performed according to the manufacturer's instructions (Beyotime technology). Briefly, brain sections fixed with 4% paraformaldehyde and permeabilized with 0.5% Trixon-100 were incubated with recombinant termination deoxynucleotidyltransferase (rTdT) for 1 h at 37℃. The fragmented DNA was labeled at the ends with Cy3-conjugated dUTP to yield red-stained nuclei, indicative of an apoptotic cell. Positive control samples were pretreated with DNase I before TUNEL staining.

Behavior test

An 'open field' test was conducted according to previously described procedures (Seibenhener and Wooten, 2015). In short, after an acclimation of 30 minutes, mice were placed individually in the middle of a 40 x 40 cm open field chamber and allowed to explore for 15 minutes freely. Throughout this period the movement trajectory of the mouse was tracked with an video camera controlled by the EthoVision XT software. Total distance traveled, motion velocity and time in movement were calculated as measures of locomotor activity.

QUANTIFICATION AND STATISTICAL ANALYSIS

All data are presented as means ± s.e.m. Statistical analysis was performed with GraphPad Prism 7. A test for normality was applied before statistical comparison. If the data conformed to a normal distribution, an unpaired two-tail Student's t-test or one-way ANOVA followed by post–hoc Tukey Kramer correction were used for comparisons between different groups; if not, the Wilcoxon rank sum test was used. Threshold p values were computed for significance levels: $*p < 0.05$, $**p < 0.01$, $***p < 0.001$.

REFERENCES

Alexander, I.E., Russell, D.W., and Miller, A.D. (1994). DNA-damaging agents greatly increase the transduction of nondividing cells by adeno-associated virus vectors. J Virol *68*, 8282-8287.

Alli, S., Figueiredo, C.A., Golbourn, B., Sabha, N., Wu, M.Y., Bondoc, A., Luck, A., Coluccia, D., Maslink, C., Smith, C.*, et al.* (2018). Brainstem blood brain barrier disruption using focused ultrasound: A demonstration of feasibility and enhanced doxorubicin delivery. J Control Release *281*, 29-41.

Angelucci, A., and Sainsbury, K. (2006). Contribution of feedforward thalamic afferents and corticogeniculate feedback to the spatial summation area of macaque V1 and LGN. J Comp Neurol *498*, 330-351.

Atasoy, D., Aponte, Y., Su, H.H., and Sternson, S.M. (2008). A FLEX switch targets Channelrhodopsin-2 to multiple cell types for imaging and long-range circuit mapping. The Journal of neuroscience : the official journal of the Society for Neuroscience *28*, 7025-7030.

Attinger, A., Wang, B., and Keller, G.B. (2017). Visuomotor Coupling Shapes the Functional Development of Mouse Visual Cortex. Cell *169*, 1291-1302.e1214.

Balakrishnan, B., and Jayandharan, G.R. (2014). Basic Biology of Adeno-Associated Virus (AAV) Vectors Used in Gene Therapy. Curr Gene Ther *14*, 86-100.

Betley, J.N., and Sternson, S.M. (2011). Adeno-associated viral vectors for mapping, monitoring, and manipulating neural circuits. Human gene therapy *22*, 669-677.

Bigotte, L., and Olsson, Y. (1982). Retrograde transport of doxorubicin (adriamycin) in peripheral nerves of mice. Neurosci Lett *32*, 217-221.

Broekman, M.L.D., Comer, L.A., Hyman, B.T., and Siena-Esteves, M. (2006). Adeno-associated virus vectors serotyped with AAV8 capsid are more efficient than AAV-1 or-2 serotypes for widespread gene delivery to the neonatal mouse brain. Neuroscience *138*, 501-510.

Cahalan, M.D., and Parker, I. (2008). Choreography of cell motility and interaction dynamics imaged by two-photon microscopy in lymphoid organs. Annu Rev Immunol *26*, 585-626.

Candolfi, M., Xiong, W.D., Yagiz, K., Liu, C.Y., Muhammad, A.K.M.G., Puntel, M., Foulad, D., Zadmehr, A., Ahlzadeh, G.E., Kroeger, K.M.*, et al.* (2010). Gene therapy-mediated delivery of targeted cytotoxins for glioma therapeutics. Proceedings of the National Academy of Sciences of the United States of America *107*, 20021-20026.

Castle, M.J., Gershenson, Z.T., Giles, A.R., Holzbaur, E.L., and Wolfe, J.H. (2014). Adeno-associated virus serotypes 1, 8, and 9 share conserved mechanisms for anterograde and retrograde axonal transport. Human gene therapy *25*, 705-720.

Chan, K.Y., Jang, M.J., Yoo, B.B., Greenbaum, A., Ravi, N., Wu, W.L., Sanchez-Guardado, L., Lois, C., Mazmanian, S.K., Deverman, B.E.*, et al.* (2017). Engineered AAVs for efficient noninvasive gene delivery to the central and peripheral nervous systems. Nat Neurosci *20*, 1172-1179.

Chien, Y.H., Lee, N.C., Tseng, S.H., Tai, C.H., Muramatsu, S.I., Byrne, B.J., and Hwu, W.L. (2017). Efficacy and safety of AAV2 gene therapy in children with aromatic L-amino acid decarboxylase deficiency: an open-label, phase 1/2 trial. Lancet Child Adolesc Health *1*, 265-273.

Choi, V.W., McCarty, D.M., and Samulski, R.J. (2006). Host cell DNA repair pathways in adeno-associated viral genome processing. J Virol *80*, 10346-10356.

Christine, C.W., Bankiewicz, K.S., Van Laar, A.D., Richardson, R.M., Ravina, B., Kells, A.P., Boot, B., Martin, A.J., Nutt, J., Thompson, M.E.*, et al.* (2019). Magnetic resonance imaging-guided phase 1 trial of putaminal AADC gene therapy for Parkinson's disease. Annals of Neurology *85*, 704-714.

Colella, P., Ronzitti, G., and Mingozzi, F. (2018). Emerging Issues in AAV-Mediated In Vivo Gene Therapy. Mol Ther-Meth Clin D *8*, 87-104.

Cruz-Martin, A., El-Danaf, R.N., Osakada, F., Sriram, B., Dhande, O.S., Nguyen, P.L., Callaway, E.M., Ghosh, A., and Huberman, A.D. (2014). A dedicated circuit links direction-selective retinal ganglion cells to the primary visual cortex. Nature *507*, 358-361.

Denk, W., Strickler, J.H., and Webb, W.W. (1990). Two-photon laser scanning fluorescence microscopy. Science (New York, NY) *248*, 73-76.

Deverman, B.E., Pravdo, P.L., Simpson, B.P., Kumar, S.R., Chan, K.Y., Banerjee, A., Wu, W.L., Yang, B., Huber, N., Pasca, S.P.*, et al.* (2016). Cre-dependent selection yields AAV variants for widespread gene transfer to the adult brain. Nat Biotechnol *34*, 204-209.

Deverman, B.E., Ravina, B.M., Bankiewicz, K.S., Paul, S.M., and Sah, D.W.Y. (2018). Gene therapy for neurological disorders: progress and prospects. Nat Rev Drug Discov *17*, 641-659.

Diester, I., Kaufman, M.T., Mogri, M., Pashaie, R., Goo, W., Yizhar, O., Ramakrishnan, C., Deisseroth, K., and Shenoy, K.V. (2011). An optogenetic toolbox designed for primates. Nature Neuroscience *14*, 387-397.

Dimidschstein, J., Chen, Q., Tremblay, R., Rogers, S.L., Saldi, G.A., Guo, L., Xu, Q., Liu, R., Lu, C., Chu, J.*, et al.* (2016). A viral strategy for targeting and manipulating interneurons across vertebrate species. Nature Neuroscience *19*, 1743-1749.
Dodiya, H.B., Bjorklund, T., Stansell, J., Mandel, R.J., Kirik, D., and Kordower, J.H. (2010). Differential Transduction Following Basal Ganglia Administration of Distinct Pseudotyped AAV Capsid Serotypes in Nonhuman Primates. Molecular Therapy *18*, 579-587.
Eldridge, M.A., Lerchner, W., Saunders, R.C., Kaneko, H., Krausz, K.W., Gonzalez, F.J., Ji, B., Higuchi, M., Minamimoto, T., and Richmond, B.J. (2016). Chemogenetic disconnection of monkey orbitofrontal and rhinal cortex reversibly disrupts reward value. Nat Neurosci *19*, 37-39.
Ferrari, F.K., Samulski, T., Shenk, T., and Samulski, R.J. (1996). Second-strand synthesis is a rate-limiting step for efficient transduction by recombinant adeno-associated virus vectors. J Virol *70*, 3227-3234.
Fisher, K.J., Gao, G.P., Weitzman, M.D., DeMatteo, R., Burda, J.F., and Wilson, J.M. (1996). Transduction with recombinant adeno-associated virus for gene therapy is limited by leading-strand synthesis. J Virol *70*, 520-532.
Gao, G.P., Alvira, M.R., Wang, L., Calcedo, R., Johnston, J., and Wilson, J.M. (2002). Novel adeno-associated viruses from rhesus monkeys as vectors for human gene therapy. Proceedings of the National Academy of Sciences of the United States of America *99*, 11854-11859.
Gilkes, J.A., Bloom, M.D., and Heldermon, C.D. (2016). Preferred transduction with AAV8 and AAV9 via thalamic administration in the MPS IIIB model: A comparison of four rAAV serotypes. Molec Genet Metab Rep *6*, 48-54.
Green, F., Samaranch, L., Zhang, H.S., Manning-Bog, A., Meyer, K., Forsayeth, J., and Bankiewicz, K.S. (2016). Axonal transport of AAV9 in nonhuman primate brain. Gene Ther *23*, 520-526.
Hadaczek, P., Eberling, J.L., Pivirotto, P., Bringas, J., Forsayeth, J., and Bankiewicz, K.S. (2010). Eight years of clinical improvement in MPTP-lesioned primates after gene therapy with AAV2-hAADC. Molecular Therapy *18*, 1458-1461.
Harvey, B.K., Airavaara, M., Hinzman, J., Wires, E.M., Chiocco, M.J., Howard, D.B., Shen, H., Gerhardt, G., Hoffer, B.J., and Wang, Y. (2011). Targeted over-expression of glutamate transporter 1 (GLT-1) reduces ischemic brain injury in a rat model of stroke. PLoS One *6*, e22135.
Hudry, E., and Vandenberghe, L.H. (2019). Therapeutic AAV Gene Transfer to the Nervous System: A Clinical Reality. Neuron *101*, 839-862.
Hwu, W.L., Muramatsu, S., Tseng, S.H., Tzen, K.Y., Lee, N.C., Chien, Y.H., Snyder, R.O., Byrne, B.J., Tai, C.H., and Wu, R.M. (2012). Gene therapy for aromatic L-amino acid decarboxylase deficiency. Sci Transl Med *4*, 134ra161.
Iacaruso, M.F., Gasler, I.T., and Hofer, S.B. (2017). Synaptic organization of visual space in primary visual cortex. Nature *547*, 449-452.
Johnston, L.C., Eberling, J., Pivirotto, P., Hadaczek, P., Federoff, H.J., Forsayeth, J., and Bankiewicz, K.S. (2009). Clinically relevant effects of convection-enhanced delivery of AAV2-GDNF on the dopaminergic nigrostriatal pathway in aged rhesus monkeys. Human gene therapy *20*, 497-510.
Ju, N.S., Jiang, R.D., Macknik, S.L., Martinez-Conde, S., and Tang, S.M. (2018). Long-term all-optical interrogation of cortical neurons in awake-behaving nonhuman primates. PLoS Biol *16*, 17.
Kanazawa, T., Urabe, M., Mizukami, H., Okada, T., Kume, A., Nishino, H., Monahan, J., Kitamura, K., Ichimura, K., and Ozawa, K. (2001). Gamma-rays enhance rAAV-mediated transgene expression and cytocidal effect of AAV-HSVtk/ganciclovir on cancer cells. Cancer gene therapy *8*, 99-106.
Kaplitt, M.G., Leone, P., Samulski, R.J., Xiao, X., Pfaff, D.W., O'Malley, K.L., and During, M.J. (1994). Long-term gene expression and phenotypic correction using adeno-associated virus vectors in the mammalian brain. Nature genetics *8*, 148-154.
Kato, S., Yamamoto, T., Iwasaki, Y., Niizuma, H., Nakamura, T., and Suzuki, J. (1988). Experimental retrograde adriamycin trigeminal sensory ganglionectomy. J Neurosurg *69*, 760-765.
Kennedy, H., and Bullier, J. (1985). A double-labeling investigation of the afferent connectivity to cortical areas V1 and V2 of the macaque monkey. The Journal of neuroscience : the official journal of the Society for Neuroscience *5*, 2815-2830.
Koda, L.Y., and Van der Kooy, D. (1983). Doxorubicin: a fluorescent neurotoxin retrogradely transported in the central nervous system. Neuroscience Letters *36*, 1-8.
Krol, A., and Feng, G.P. (2018). Windows of opportunity: timing in neurodevelopmental disorders. Curr Opin Neurobiol *48*, 59-63.
Levis, B.E., Binkley, P.F., and Shapiro, C.L. (2017). Cardiotoxic effects of anthracycline-based therapy: what is the evidence and what are the potential harms? Lancet Oncol *18*, E445-E456.
Li, M., Liu, F., Jiang, H.F., Lee, T.S., and Tang, S.M. (2017). Long-Term Two-Photon Imaging in Awake Macaque Monkey. Neuron *93*, 1049-1057.e1043.
Lu, H., Wang, Y., He, X., Yuan, F., Lin, X., Xie, B., Tang, G., Huang, J., Tang, Y., Jin, K.*, et al.* (2012). Netrin-1 hyperexpression in mouse brain promotes angiogenesis and long-term neurological recovery after transient focal ischemia. Stroke *43*, 838-843.
Maes, M.E., Colombo, G., Schulz, R., and Siegert, S. (2019). Targeting microglia with lentivirus and AAV: Recent advances and remaining challenges. Neuroscience Letters *707*, 134310.
Maheshri, N., Koerber, J.T., Kaspar, B.K., and Schaffer, D.V. (2006). Directed evolution of adeno-associated virus yields enhanced gene delivery vectors. Nat Biotechnol *24*, 198-204.
Maini, C.L., Sciuto, R., Ferraironi, A., Vici, P., Tofani, A., Festa, A., Conti, F., and Lopez, M. (1997). Clinical relevance of radionuclide angiography and antimyosin immunoscintigraphy for risk assessment in epirubicin cardiotoxicity. J Nucl Cardiol *4*, 502-508.

Mainprize, T., Lipsman, N., Huang, Y., Meng, Y., Bethune, A., Ironside, S., Heyn, C., Alkins, R., Trudeau, M., Sahgal, A., *et al.* (2019). Blood-Brain Barrier Opening in Primary Brain Tumors with Non-invasive MR-Guided Focused Ultrasound: A Clinical Safety and Feasibility Study. Scientific Reports *9*, 321.
Markakis, E.A., Vives, K.P., Bober, J., Leichtle, S., Leranth, C., Beecham, J., Elsworth, J.D., Roth, R.H., Samulski, R.J., and Redmond, D.E. (2010). Comparative Transduction Efficiency of AAV Vector Serotypes 1-6 in the Substantia Nigra and Striatum of the Primate Brain. Molecular Therapy *18*, 588-593.
Markov, N.T., Ercsey-Ravasz, M.M., Ribeiro Gomes, A.R., Lamy, C., Magrou, L., Vezoli, J., Misery, P., Falchier, A., Quilodran, R., Gariel, M.A., *et al.* (2014). A weighted and directed interareal connectivity matrix for macaque cerebral cortex. Cerebral Cortex *24*, 17-36.
Masamizu, Y., Okada, T., Ishibashi, H., Takeda, S., Yuasa, S., and Nakahara, K. (2010). Efficient gene transfer into neurons in monkey brain by adeno-associated virus 8. Neuroreport *21*, 447-451.
Masamizu, Y., Okada, T., Kawasaki, K., Ishibashi, H., Yuasa, S., Takeda, S., Hasegawa, I., and Nakahara, K. (2011). Local and retrograde gene transfer into primate neuronal pathways via adeno-associated virus serotype 8 and 9. Neuroscience *193*, 249-258.
McCarty, D.M., Fu, H., Monahan, P.E., Toulson, C.E., Naik, P., and Samulski, R.J. (2003). Adeno-associated virus terminal repeat (TR) mutant generates self-complementary vectors to overcome the rate-limiting step to transduction in vivo. Gene Ther *10*, 2112-2118.
McCarty, D.M., Monahan, P.E., and Samulski, R.J. (2001). Self-complementary recombinant adeno-associated virus (scAAV) vectors promote efficient transduction independently of DNA synthesis. Gene Ther *8*, 1248-1254.
Mehta, A.M., Sonabend, A.M., and Bruce, J.N. (2017). Convection-Enhanced Delivery. Neurotherapeutics *14*, 358-371.
Mendell, J.R., Al-Zaidy, S., Shell, R., Arnold, W.D., Rodino-Klapac, L.R., Prior, T.W., Lowes, L., Alfano, L., Berry, K., Church, K., *et al.* (2017). Single-Dose Gene-Replacement Therapy for Spinal Muscular Atrophy. New England Journal of Medicine *377*, 1713-1722.
Mendoza, S.D., El-Shamayleh, Y., and Horwitz, G.D. (2017). AAV-mediated delivery of optogenetic constructs to the macaque brain triggers humoral immune responses. Journal of Neurophysiology *117*, 2004.
Meredith, R.M. (2015). Sensitive and critical periods during neurotypical and aberrant neurodevelopment: A framework for neurodevelopmental disorders. Neurosci Biobehav R *50*, 180-188.
Mittermeyer, G., Christine, C.W., Rosenbluth, K.H., Baker, S.L., Starr, P., Larson, P., Kaplan, P.L., Forsayeth, J., Aminoff, M.J., and Bankiewicz, K.S. (2012). Long-Term Evaluation of a Phase 1 Study of AADC Gene Therapy for Parkinson's Disease. Human gene therapy *23*, 377-381.
Monahan, P.E., Sun, J., Gui, T., Hu, G., Hannah, W.B., Wichlan, D.G., Wu, Z., Grieger, J.C., Li, C., Suwanmanee, T., *et al.* (2015). Employing a gain-of-function factor IX variant R338L to advance the efficacy and safety of hemophilia B human gene therapy: preclinical evaluation supporting an ongoing adeno-associated virus clinical trial. Human gene therapy *26*, 69-81.
Mross, K., Maessen, P., Vandervijgh, W.J.F., Gall, H., Boven, E., and Pinedo, H.M. (1988). Pharmacokinetics and Metabolism of Epidoxorubicin and Doxorubicin in Humans. J Clin Oncol *6*, 517-526.
Naldini, L. (2015). Gene therapy returns to centre stage. Nature *526*, 351-360.
Nassi, J.J., Cepko, C.L., Born, R.T., and Beier, K.T. (2015). Neuroanatomy goes viral! Frontiers in Neuroanatomy *9*.
Nathanson, J.L., Yanagawa, Y., Obata, K., and Callaway, E.M. (2009). Preferential labeling of inhibitory and excitatory cortical neurons by endogenous tropism of adeno-associated virus and lentivirus vectors. Neuroscience *161*, 441-450.
Nicolson, S.C., Li, C.W., Hirsch, M.L., Setola, V., and Samulski, R.J. (2016). Identification and Validation of Small Molecules That Enhance Recombinant Adeno-associated Virus Transduction following High-Throughput Screens. J Virol *90*, 7019-7031.
Oh, S.W., Harris, J.A., Ng, L., Winslow, B., Cain, N., Mihalas, S., Wang, Q., Lau, C., Kuan, L., Henry, A.M., *et al.* (2014). A mesoscale connectome of the mouse brain. Nature *508*, 207-214.
Oligschlager, S., Xu, T., Baczkowski, B.M., Falkiewicz, M., Falchier, A., Linn, G., and Margulies, D.S. (2019). Gradients of connectivity distance in the cerebral cortex of the macaque monkey. Brain Struct Funct *224*, 925-935.
Pakan, J.M., Lowe, S.C., Dylda, E., Keemink, S.W., Currie, S.P., Coutts, C.A., and Rochefort, N.L. (2016). Behavioral-state modulation of inhibition is context-dependent and cell type specific in mouse visual cortex. eLife *5*.
Parekh, R., and Ascoli, G.A. (2013). Neuronal morphology goes digital: a research hub for cellular and system neuroscience. Neuron *77*, 1017-1038.
Peel, A.L., Zolotukhin, S., Schrimsher, G.W., Muzyczka, N., and Reier, P.J. (1997). Efficient transduction of green fluorescent protein in spinal cord neurons using adeno-associated virus vectors containing cell type-specific promoters. Gene Ther *4*, 16-24.
Perkel, D.J., Bullier, J., and Kennedy, H. (1986). Topography of the afferent connectivity of area 17 in the macaque monkey: a double-labelling study. Journal of Comparative Neurology *253*, 374-402.
Prasad, K.M.R., Xu, Y.Q., Yang, Z.Q., Toufektsian, M.C., Berr, S.S., and French, B.A. (2007). Topoisomerase inhibition accelerates gene expression after adeno-associated virus-mediated gene transfer to the mammalian heart. Molecular Therapy *15*, 764-771.
Rabinowitz, J.E., Bowles, D.E., Faust, S.M., Ledford, J.G., Cunningham, S.E., and Samulski, R.J. (2004). Cross-dressing the virion: the transcapsidation of adeno-associated virus serotypes functionally defines subgroups. J Virol *78*, 4421-4432.
Ran, F.A., Cong, L., Yan, W.X., Scott, D.A., Gootenberg, J.S., Kriz, A.J., Zetsche, B., Shalem, O., Wu, X.B., Makarova, K.S., *et al.* (2015). In vivo genome editing using Staphylococcus aureus Cas9. Nature *520*, 186-U198.

Rockland, K.S., and Pandya, D.N. (1979). Laminar origins and terminations of cortical connections of the occipital lobe in the rhesus monkey. Brain research *179*, 3-20.
Rockland, K.S., and Virga, A. (1989). Terminal arbors of individual "feedback" axons projecting from area V2 to V1 in the macaque monkey: a study using immunohistochemistry of anterogradely transported Phaseolus vulgaris-leucoagglutinin. J Comp Neurol *285*, 54-72.
Rubart, M. (2004). Two-photon microscopy of cells and tissue. Circ Res *95*, 1154-1166.
Russell, D.W., Alexander, I.E., and Miller, A.D. (1995). DNA synthesis and topoisomerase inhibitors increase transduction by adeno-associated virus vectors. Proceedings of the National Academy of Sciences of the United States of America *92*, 5719-5723.
Samaranch, L., Salegio, E.A., San Sebastian, W., Kells, A.P., Foust, K.D., Bringas, J.R., Lamarre, C., Forsayeth, J., Kaspar, B.K., and Bankiewicz, K.S. (2012). Adeno-associated virus serotype 9 transduction in the central nervous system of nonhuman primates. Human gene therapy *23*, 382-389.
Sauter, K.A.D., Wood, L.J., Wong, J., Iordanov, M., and Magun, B.E. (2011). Doxorubicin and daunorubicin induce processing and release of interleukin-1 beta through activation of the NLRP3 inflammasome. Cancer Biol Ther *11*, 1008-1016.
Sehara, Y., Fujimoto, K.I., Ikeguchi, K., Katakai, Y., Ono, F., Takino, N., Ito, M., Ozawa, K., and Muramatsu, S.I. (2017). Persistent Expression of Dopamine-Synthesizing Enzymes 15 Years After Gene Transfer in a Primate Model of Parkinson's Disease. Hum Gene Ther Clin Dev *28*, 74-79.
Sehara, Y., Inaba, T., Urabe, T., Kurosaki, F., Urabe, M., Kaneko, N., Shimazaki, K., Kawai, K., and Mizukami, H. (2018). Survivin overexpression via adeno-associated virus vector Rh10 ameliorates ischemic damage after middle cerebral artery occlusion in rats. Eur J Neurosci *48*, 3466-3476.
Seibenhener, M.L., and Wooten, M.C. (2015). Use of the Open Field Maze to measure locomotor and anxiety-like behavior in mice. J Vis Exp.
Seidemann, E., Chen, Y., Bai, Y., Chen, S.C., Mehta, P., Kajs, B.L., Geisler, W.S., and Zemelman, B.V. (2016). Calcium imaging with genetically encoded indicators in behaving primates. Elife *5*.
Shimazaki, K., Urabe, M., Monahan, J., Ozawa, K., and Kawai, N. (2000). Adeno-associated virus vector-mediated bcl-2 gene transfer info post-ischemic gerbil brain in vivo: prospects for gene therapy of ischemia-induced neuronal death. Gene Ther *7*, 1244-1249.
Squirrell, J.M., Wokosin, D.L., White, J.G., and Bavister, B.D. (1999). Long-term two-photon fluorescence imaging of mammalian embryos without compromising viability. Nat Biotechnol *17*, 763-767.
Srivastava, A. (2016). In vivo tissue-tropism of adeno-associated viral vectors. Curr Opin Virol *21*, 75-80.
Sun, S., and Schaffer, D.V. (2018). Engineered viral vectors for functional interrogation, deconvolution, and manipulation of neural circuits. Curr Opin Neurobiol *50*, 163-170.
Svoboda, K., and Yasuda, R. (2006). Principles of two-photon excitation microscopy and its applications to neuroscience. Neuron *50*, 823-839.
Tacar, O., Sriamornsak, P., and Dass, C.R. (2013). Doxorubicin: an update on anticancer molecular action, toxicity and novel drug delivery systems. The Journal of pharmacy and pharmacology *65*, 157-170.
Tardieu, M., Zerah, M., Husson, B., de Bournonville, S., Deiva, K., Adamsbaum, C., Vincent, F., Hocquemiller, M., Broissand, C., Furlan, V.*, et al.* (2014). Intracerebral administration of adeno-associated viral vector serotype rh.10 carrying human SGSH and SUMF1 cDNAs in children with mucopolysaccharidosis type IIIA disease: results of a phase I/II trial. Human gene therapy *25*, 506-516.
Tervo, D.G.R., Hwang, B.Y., Viswanathan, S., Gaj, T., Lavzin, M., Ritola, K.D., Lindo, S., Michael, S., Kuleshova, E., Ojala, D.*, et al.* (2016). A Designer AAV Variant Permits Efficient Retrograde Access to Projection Neurons. Neuron *92*, 372-382.
Tian, L., Akerboom, J., Schreiter, E.R., and Looger, L.L. (2012). Neural activity imaging with genetically encoded calcium indicators. Prog Brain Res *196*, 79-94.
Tian, L., Hires, S.A., Mao, T., Huber, D., Chiappe, M.E., Chalasani, S.H., Petreanu, L., Akerboom, J., McKinney, S.A., Schreiter, E.R.*, et al.* (2009). Imaging neural activity in worms, flies and mice with improved GCaMP calcium indicators. Nature methods *6*, 875-881.
Vela, J.M., Yanez, A., Gonzalez, B., and Castellano, B. (2002). Time course of proliferation and elimination of microglia/macrophages in different neurodegenerative conditions. Journal of neurotrauma *19*, 1503-1520.
Vite, C.H., Passini, M.A., Haskins, M.E., and Wolfe, J.H. (2003). Adeno-associated virus vector-mediated transduction in the cat brain. Gene Ther *10*, 1874-1881.
Wang, D., Tai, P.W.L., and Gao, G.P. (2019). Adeno-associated virus vector as a platform for gene therapy delivery. Nature Reviews Drug Discovery *18*, 358-378.
Wang, X.J., and Kennedy, H. (2016). Brain structure and dynamics across scales: in search of rules. Curr Opin Neurobiol *37*, 92-98.
Watakabe, A., Ohtsuka, M., Kinoshita, M., Takaji, M., Isa, K., Mizukami, H., Ozawa, K., Isa, T., and Yamamori, T. (2015). Comparative analyses of adeno-associated viral vector serotypes 1, 2, 5, 8 and 9 in marmoset, mouse and macaque cerebral cortex. Neurosci Res *93*, 144-157.
Weller, R.E., and Kaas, J.H. (1983). Retinotopic pattern of connections of area 17 with visual areas V-II and MT in macaque monkeys. Journal of Comparative Neurology *220*, 253-279.
Yan, Z.Y., Zak, R., Zhang, Y.L., Ding, W., Godwin, S., Munson, K., Peluso, R., and Engelhardt, J.F. (2004). Distinct classes of

proteasome-modulating agents cooperatively augment recombinant adeno-associated virus type 2 and type 5-mediated transduction from the apical surfaces of human airway epithelia. J Virol *78*, 2863-2874.
Yang, B., Li, S.Y., Wang, H.Y., Guo, Y.S., Gessler, D.J., Cao, C.Y., Su, Q., Kramer, J., Zhong, L., Ahmed, S.S.*, et al.* (2014). Global CNS Transduction of Adult Mice by Intravenously Delivered rAAVrh.8 and rAAVrh.10 and Nonhuman Primates by rAAVrh.10. Molecular Therapy *22*, 1299-1309.
Yang, L., Jiang, J., Drouin, L.M., Agbandje-McKenna, M., Chen, C., Qiao, C., Pu, D., Hu, X., Wang, D.Z., Li, J.*, et al.* (2009). A myocardium tropic adeno-associated virus (AAV) evolved by DNA shuffling and in vivo selection. Proceedings of the National Academy of Sciences of the United States of America *106*, 3946-3951.
Yang, W., Carrasquillo, Y., Hooks, B.M., Nerbonne, J.M., and Burkhalter, A. (2013). Distinct balance of excitation and inhibition in an interareal feedforward and feedback circuit of mouse visual cortex. The Journal of neuroscience : the official journal of the Society for Neuroscience *33*, 17373-17384.
Yazdan-Shahmorad, A., Tian, N., Kharazia, V., Samaranch, L., Kells, A., Bringas, J., He, J.W., Bankiewicz, K., and Sabes, P.N. (2018). Widespread optogenetic expression in macaque cortex obtained with MR-guided, convection enhanced delivery (CED) of AAV vector to the thalamus. J Neurosci Methods *293*, 347-358.
Zhang, S., Xu, M., Chang, W.-C., Ma, C., Hoang Do, J.P., Jeong, D., Lei, T., Fan, J.L., and Dan, Y. (2016). Organization of long-range inputs and outputs of frontal cortex for top-down control. Nature Neuroscience *19*, 1733-1742.
Zhang, S., Xu, M., Kamigaki, T., Hoang Do, J.P., Chang, W.C., Jenvay, S., Miyamichi, K., Luo, L., and Dan, Y. (2014). Selective attention. Long-range and local circuits for top-down modulation of visual cortex processing. Science (New York, NY) *345*, 660-665.
Zhang, S.H., Wu, J.H., Wu, X.B., Xu, P., Tian, Y.H., Yi, M.Y., Liu, X.J., Dong, X.Y., Wolf, F., Li, C.Y.*, et al.* (2012). Enhancement of rAAV2-Mediated Transgene Expression in Retina Cells In Vitro and In Vivo by Coadministration of Low-Dose Chemotherapeutic Drugs. Invest Ophth Vis Sci *53*, 2675-2684.
Zhang, T., Hu, J., Ding, W., and Wang, X.M. (2009). Doxorubicin augments rAAV-2 transduction in rat neuronal cells. Neurochem Int *55*, 521-528.
Zhong, L., Li, B., Mah, C.S., Govindasamy, L., Agbandje-McKenna, M., Cooper, M., Herzog, R.W., Zolotukhin, I., Warrington, K.H., Jr., Weigel-Van Aken, K.A.*, et al.* (2008). Next generation of adeno-associated virus 2 vectors: point mutations in tyrosines lead to high-efficiency transduction at lower doses. Proceedings of the National Academy of Sciences of the United States of America *105*, 7827-7832.
Zmarz, P., and Keller, Georg B. (2016). Mismatch Receptive Fields in Mouse Visual Cortex. Neuron *92*, 766-772.